Contrib Mineral Petrol (2007) 153:29–53
DOI 10.1007/s00410-006-0131-2

ORIGINAL PAPER

New constraints on the origin and age of Variscan eclogitic rocks (Ligurian Alps, Italy)

Folco Giacomini · Roberto Braga · Massimo Tiepolo · Riccardo Tribuzio

Received: 30 May 2006 / Accepted: 3 August 2006 / Published online: 8 September 2006

Abstract Gabbro and eclogite boudins are preserved within the amphibolites of the composite para- and ortho-gneiss Variscan basement of the Savona Crystalline Massif (Ligurian Briançonnais, Italy). Whole rock trace element patterns, low initial εNd (+5.4 to +8.8) data and trace element analyses on relict igneous clinopyroxene revealed that the mafic rocks were derived from depleted mantle melts, which most likely underwent crustal contamination during emplacement. Gabbros have a cumulus origin controlled by clinopyroxene and plagioclase segregation, whereas the eclogites represent evolved melts. U-Pb and trace element micro-analyses on zircons separated from one amphibolitised gabbro and one eclogite help to constrain coeval ages at ~468 Ma for their igneous protoliths. The occurrence of a few inherited zircons confirms the involvement of a crustal component in the petrogenesis of the mafic rocks. In the eclogite, concordant zircon ages younger than the protolith age testify to metamorphic re-crystallisation (or new growth) from about 420 to 305 Ma. Zircon textures and trace element compositions indicate that eclogite facies metamorphism occurred 392–376 Ma ago. The younger zircon portions yielding a mean Concordia age of 333 ± 7 Ma are related to equilibration or new growth during the post-eclogite, amphibolite-facies equilibration.

Keywords Variscan · Eclogite · Gabbro · Zircon geochronology · LA-ICP-MS

Communicated by J. Hoefs.

F. Giacomini (✉)
Dipartimento di Scienze della Terra, Università di Siena, via Laterina 8, Siena, Italy
e-mail: giacomini@unisi.it

R. Braga
Dipartimento di Scienze della Terra e Geologico-Ambientali, Università di Bologna, P.za San Donato 1, Bologna, Italy

M. Tiepolo
CNR-IGG Unità di Pavia, via Ferrata 1, Pavia, Italy

R. Tribuzio
Dipartimento di Scienze della Terra, Università di Pavia, via Ferrata 1, Pavia, Italy

Introduction

Eclogites and amphibolites are widespread in sections of the Variscan basement exposed in the Alps and adjoining areas (Provence, Corsica and Sardinia). These basement slices are characterised by similar lithological units recording analogous metamorphic events. Eclogitic rocks usually occur in the cores of mafic boudins associated with amphibolite facies paragneisses (often migmatitic) and orthogneisses. There is a general consensus that most of these mafic rocks derive from Cambro-Ordovician igneous protoliths (Paquette et al. 1989; Rubatto et al. 2001; Schaltegger et al. 2003; Cortesogno et al. 2004; Palmeri et al. 2004; Giacomini et al. 2005), while the age of the high-pressure metamorphic overprint is debated.

Eclogite-facies rocks cropping out in the Gotthard massif were dated to 460–470 Ma by combining SHRIMP I data on zircons and the Sm-Nd isochron on whole rocks and garnets (Gebauer et al. 1988, Gebauer 1993). In the external Alpine Massifs of the western Alps, the eclogite-facies equilibration was instead ascribed to the Silurian (425–395 Ma) on the basis of

intercept ages from conventional U/Pb analyses on zircons (Paquette et al. 1989). A not better defined ''high-grade event'' in the eclogites from northern Sardinia was dated to 403 ± 4 Ma on the basis of conventional U-Pb analyses on a metamorphic-looking zircon population (Cortesogno et al. 2004). Despite several other recent attempts (Rubatto et al. 2001; Palmeri et al. 2004; Giacomini et al. 2005), no other data are currently available for the timing of the eclogite facies overprint in the western Alps and Sardinia.

In this work, metagabbros and eclogites from the Savona Crystalline Massif in the Ligurian Alps, Italy (Fig. 1a, b) were analysed for major, trace element and Nd isotope compositions. The in situ LA-ICPMS trace element composition of relict igneous clinopyroxene from metagabbros was also determined. The U-Pb isotope and trace element composition of zircons from one gabbro sample and one eclogite were analysed in situ (LA-ICPMS) for geochronological purposes. The timing of pre-Alpine metamorphism in the Ligurian Briançonnais basement is poorly constrained. Published geochronological data only constrain the late, widespread amphibolite facies re-equilibration, which is thought to be coeval with the development of the main regional foliation. In particular, Rb/Sr and Ar-Ar data indicate that the amphibolite-facies metamorphism of the paragneisses and orthogneisses in the Ligurian basement occurred between 327 and 297 Ma (Del Moro et al. 1981; Barbieri et al. 2003).

The principal goal of this study was to define the age of the still undated igneous protoliths and the high-pressure eclogitic overprint in the mafic rocks of this sector of the Variscan belt and to propose strategies for the interpretation of U/Pb zircon data in complex metamorphic systems. The study of mafic rocks cropping out in the Savona Crystalline Massif through a combination of in situ or bulk isotope data and geochemical analysis has provided new data for reconstructing the magmatic and tectono-metamorphic history of the basement of the Briançonnais zone. The comparison with published literature data on neighbouring southwest European Variscan units permitted a better understanding of the geodynamic evolution of the collisional belt.

Geological setting and field relations

The Savona Crystalline Massif (Fig. 1b) belongs to the Ligurian Briançonnais domain, a stack of pre-Alpine sedimentary sequences and basement slices thought to

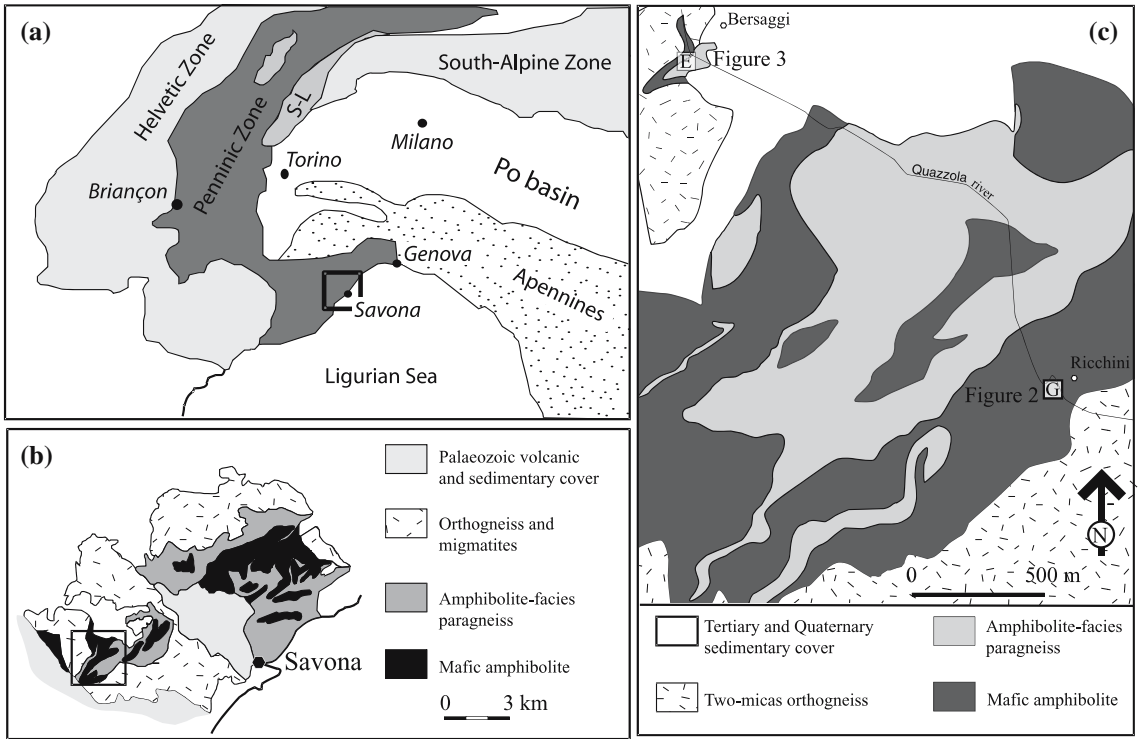

Fig. 1 **a** Tectonic map of the Western and Central Alps. The Penninic Zone comprises the Briançonnais Zone (or Grand Saint Bernard nappe system), which overthrust the Helvetic Domain. **b** Geological map of the Savona Crystalline Massif. **c** Geological sketch map of the Val Quazzola area. E, eclogite-facies relics; G, gabbro relics

represent the Mesozoic passive margin of the European continent (Vanossi et al. 1984). The Savona Crystalline Massif comprises a strongly deformed mafic amphibolite-paragneiss complex in tectonic contact with orthogneisses. Locally, the amphibolites retain relics of gabbro and of eclogite facies assemblages of unknown age (Messiga 1987; Messiga et al. 1992; Cortesogno et al. 1993, Gaggero et al. 2004). Orthogneisses and paragneisses record white mica whole-rock and biotite whole-rock Rb-Sr ages of 327–297 Ma, which were attributed to cooling under amphibolite facies conditions (Del Moro et al. 1981). Ar/Ar ages of 311–302 Ma were obtained for white micas separated from paragneiss pebbles of the Tertiary molasse overlying the basement (Barbieri et al. 2003). A white mica separate from a paragneiss associated with the amphibolitised gabbros yielded a Rb/Sr cooling age of 308 ± 11 Ma (Del Moro et al. 1982). The Alpine metamorphic overprint does not exceed greenschist facies conditions (Messiga 1987; Messiga et al. 1992; Cortesogno et al. 1993, Cortesogno et al. 1997).

The study area comprises the valley of the Quazzola stream between Bersaggi and Richini villages (Fig. 1c). Undeformed bodies of either gabbro or partially retrogressed eclogite occur within the mafic amphibolites along the bed of the torrent. Gabbro- and eclogite-relics are not associated in the same outcrop. Near Richini village the mafic amphibolites contain decametre-scale metagabbro boudins. The gabbroic rocks preserve an igneous layering defined by modal and/or grain-size variations in plagioclase and clinopyroxene, the latter showing coronas of hornblende. Decimetre-scale layers of melagabbro are sometimes present. A coarse-grained fels rich in staurolite, garnet and magnetite occurs as a meter-scale lens within a deformed and amphibolitised gabbro. This lens is SiO_2-poor and Al_2O_3-rich (both ~30 wt%) and most likely related to digestion of crustal rocks by the basic magma (Braga and Tribuzio 1999). The contact between this enclave and the host amphibolitised gabbro is marked by the appearance of magnetite + quartz in the amphibolite paragenesis. Near Bersaggi village, about two kilometres northwest of the previous location, retrogressed eclogites form metre-scale, non-foliated domains within banded amphibolites. In the outcrop, the retrogressed eclogites show subhedral to anhedral garnet porphyroblasts (up to 1 cm in diameter) set in a light grey, fine-grained foliated matrix. Garnet porphyroblasts commonly bear coronas of dark-green amphibole aggregates. The transition from retrogressed eclogites to banded amphibolites is marked by a gradual decrease in the garnet-amphibole modal ratio and a progressive disappearing of the light matrix.

Methods

Whole rock major, trace element and Nd isotope compositions were determined at Activation Laboratories (Ancaster, ON, Canada). Major and trace element analyses (Table 1) were carried out by ICP-MS; precision and accuracy are generally estimated to be better than 10%. Nd isotope analyses (Table 2) were performed using a Finnigan MAT 261 8-collector mass-spectrometer in static mode. Powdered samples were dissolved in a Hf-HNO_3-HCl mixture. $^{143}Nd/^{144}Nd$ ratios are relative to the value of 0.511860 for the La Jolla standard.

The trace element composition of igneous clinopyroxene was determined by laser ablation (LA)-ICP-MS at the CNR-Istituto di Geoscienze e Georisorse– Unità di Pavia. The reader can refer to Tiepolo et al. (2003) for analytical details The LA-ICP-MS instrument couples a Nd:YAG laser operating at 213 nm with a double focusing sector field ICP mass spectrometer type Element I from Thermo. The laser was operated at a repetition rate of 10 Hz, with a spot diameter of 20–40 μm and a pulse energy of about 0.01–0.03 mJ, respectively. Data reduction was performed using the software package ''Glitter'' (van Achterberg et al. 2001). NIST SRM 612 was used as the external standard. ^{44}Ca or ^{29}Si were adopted as the internal standards, depending on the mineral composition. Precision and accuracy, assessed against the BCR-2 USGS reference glass, are better than 6% relative.

Zircon grains for the geochronological characterisation were separated using standard techniques starting from a sieved rock fraction of 60–250 microns; grains were mounted in epoxy resin and then polished down using 0.25 micron diamond paste. Pb geochronology of zircons was carried out at the CNR-IGG-Unità di Pavia using an ArF excimer laser ablation microprobe operating at 193 nm (Geolas200Q-Micrrolas) coupled with the previously described HR-ICPMS (Element-ThermoFinnigan). Laser was operated at 5 Hz, fluency was set at 12 J/cm^{2}and the spot size to 25 or 10 μm according to the internal complexity of zircon. The method is basically that described in Tiepolo (2003) and in Miller et al. (2006). The signals of masses ^{202}Hg, ^{204}Pb, ^{206}Pb, ^{207}Pb, ^{232}Th and ^{238}U were acquired in magnetic mode. The ^{235}U signal is calculated from ^{238}U on the basis of the ratio $^{238}U/^{235}U = 137.88$. Approximately 60 s of background and at least 30 s of ablation signal from zircon were acquired. The time resolved signal and U/Pb ratios were carefully inspected in order to detect perturbations related to inclusions, cracks or mixing between different age domains. Zircon showing detectable

Table 1 Bulk major and trace element compositions of selected samples

Lithotype	Gabbro	Gabbro	Gabbro	Eclogite	Eclogite	Eclogite	Eclogite
Sample	GBSV3	GBSV2	GBSV4	SV6	SV1	SV2	SV4
% Wt							
SiO_2	47.88	48.40	49.17	48.94	49.45	49.72	50.13
TiO_2	0.27	0.23	0.27	1.26	1.93	1.40	1.28
Al_2O_3	16.26	16.27	17.42	15.79	13.64	15.55	15.75
Fe_2O_3	1.15	1.10	0.80	1.45	2.10	1.50	1.64
FeO	5.88	5.56	4.17	7.42	10.55	7.67	8.46
MnO	0.13	0.13	0.10	0.16	0.21	0.16	0.15
MgO	11.30	10.21	9.11	8.33	6.08	8.29	7.89
CaO	12.93	13.27	15.00	10.91	10.83	11.57	10.12
Na_2O	1.88	2.00	1.98	3.30	2.86	2.51	3.46
K_2O	0.20	0.11	0.11	0.91	0.22	0.22	0.24
P_2O_5	<D.L.	<D.L.	0.02	0.13	0.17	0.13	0.10
LOI	2.69	2.54	1.73	1.91	1.16	1.27	1.40
Sum	100.56	99.82	99.87	100.51	99.20	99.99	100.62
mg#	0.77	0.77	0.80	0.67	0.51	0.66	0.62
ppm							
Ba	65	125	52	219	75	76	17
Rb	8	3	1	30	5	6	5
Sr	201	179	197	135	97	186	139
Cs	0.3	0.2	0.1	1	0.1	0.3	0.2
Ga	11	12	13	16	20	18	16
Sc	40	36	47	39	47	43	39
Ta	<D.L.	0.02	<D.L.	0.15	0.19	0.2	0.09
Nb	<D.L.	0.4	<D.L.	2.4	3	3	1.7
Hf	0.3	0.3	0.3	2.2	3.8	2.6	2.2
Zr	10	<D.L.	4	81	124	93	74
Y	6.4	8	7.5	26.7	52.6	31	27.6
Th	0.07	0.17	0.08	0.22	0.26	0.27	0.22
U	0.02	0.08	0.05	0.16	0.35	0.12	0.76
Cr	430	100	640	250	<D.L.	300	270
Ni	100	80	80	100	30	70	90
Co	42	44	38	34	44	45	41
V	136	110	138	263	402	259	300
Cu	110	120	80	60	40	170	60
Pb	<D.L.	8	<D.L.	7	<D.L.	13	<D.L.
Zn	<D.L.	30	<D.L.	90	60	80	80
La	0.79		0.65	3.90	4.63	4.54	3.12
Ce	1.82	1.69	1.59	10.90	14.40	12.50	9.00
Pr	0.31	0.39	0.28	1.83	2.37	1.95	1.57
Nd	1.95	2.15	1.81	10.10	13.30	10.50	9.29
Sm	0.71	0.76	0.72	3.23	4.55	3.47	3.07
Eu	0.43	0.52	0.46	1.20	1.62	1.39	1.12
Gd	0.91	0.99	1.00	4.21	6.69	4.58	4.07
Tb	0.18	0.20	0.20	0.75	1.31	0.84	0.76
Dy	1.17	1.28	1.30	4.51	8.54	5.19	4.87
Ho	0.24	0.26	0.27	0.94	1.79	1.05	1.00
Er	0.69	0.76	0.75	2.75	5.50	3.04	2.95
Tm	0.10	0.11	0.11	0.41	0.85	0.44	0.45
Yb	0.63	0.65	0.65	2.64	5.35	2.73	2.90
Lu	0.09	0.10	0.10	0.39	0.76	0.41	0.42

mg# = molar (MgO/(MgO+FeO))

<*D.L.* below detection limits

common Pb (from the ^{204}Pb count rate) were neglected. The laser induced U-Pb fractionation was corrected adopting a matrix matched external standard (zircon 91500) and considering the same spot size and integration interval on the unknown and the standard zircon. Data reduction, isotope ratio and apparent age calculation was carried out with the GLITTER software (Macquarie Research Ltd, 2001) developed by Van Achterbergh et al. (2001). Concordia plot and concordant age values were calculated using the ISOPLOT/EX software by Ludwig (1999). In each analytical run zircon 02123 (Ketchum et al. 2001) was

Table 2 Isotope Nd composition and $^{147}Sm/^{144}Nd$ ratios of the selected samples

	Sample	$^{143}Nd/^{144}Nd_{(0)}$	2SE	$^{147}Sm/^{144}Nd$	$\varepsilon_{Nd}(0)$	$^{143}Nd/^{144}Nd_{(470)}$	$^{143}Nd/^{144}Nd_{(CHUR,470)}$	$\varepsilon_{Nd}(470)$
Gabbro	GBSV2	0.512965	0.000011	0.214	6.38	0.512307	0.512032	5.4
	GBSV4	0.513121	0.000008	0.241	9.42	0.512380	0.512032	6.8
	GBSV3	0.513160	0.000006	0.220	10.18	0.512482	0.512032	8.8
		$^{143}Nd/^{144}Nd_{(0)}$	2SE	$^{147}Sm/^{144}Nd$	$\varepsilon_{Nd}(0)$	$^{143}Nd/^{144}Nd_{(460)}$	$^{143}Nd/^{144}Nd_{(CHUR,460)}$	$\varepsilon_{Nd}(460)$
Eclogite	SV2	0.513004	0.000004	0.200	7.14	0.512402	0.512045	7.0
	SV6	0.513025	0.000004	0.193	7.55	0.512442	0.512045	7.8
	SV1	0.513129	0.000004	0.207	9.58	0.512506	0.512045	9.0
	SV4	0.513119	0.000006	0.200	9.38	0.512517	0.512045	9.2

analysed as unknown as quality control and average accuracy is estimated close to 1%.

LAM-ICP MS trace element analyses were carried out on selected age-concordant zircons according to the method for trace element determination described above but using the 193 nm laser source. Ablation spots about 25 μm in diameter were located near the spots of U-Pb analyses.

Petrology of selected samples

This study determined the whole rock major and trace element chemistry and Sm-Nd composition of three metagabbro samples (GBSV2, GBSV3 and GBSV4) and four retrogressed eclogites (SV1, SV2, SV3 and SV4). The selected metagabbros preserve igneous textures and fresh clinopyroxene of igneous origin and record the lowest degree of amphibolite-facies recrystallisation. An additional metagabbro sample (GBSV1) was chosen for zircon separation. The retrogressed eclogites were selected in order to avoid samples with a greater degree of retrograde amphibolite-facies recrystallization (e.g., amphibole aggregates forming pseudomorphs after garnet).

Gabbros

The gabbroic rocks (Fig. 2) consist of euhedral plagioclase (about 55 vol%), subhedral to poikilitic clinopyroxene and a completely altered mafic mineral. The latter is replaced by rounded aggregates of colourless amphibole, which make up about 10 vol % of the rocks and have been interpreted as pseudomorphs after olivine. In all samples, clinopyroxene is rimmed by fine-grained aggregates of green amphibole and minor plagioclase. Accessory Fe-sulphides occur as inclusions within the major minerals. Scarce pseudomorphs of rutile and titanite interstitial to the major minerals suggest the presence of accessory Fe-Ti-oxide phases in the original igneous assemblage. Rare plagioclase grains with igneous texture are preserved and have an anorthite content of 60–63 mol %. Plagioclase is commonly altered to fine-grained aggregates of albite and epidote. The mg# value [Mg/(Mg+Fe*)] of clinopyroxene ranges from 0.76 to 0.89. The Al and Cr contents in clinopyroxenes generally decrease with decreasing mg#, whereas Mn increases.

Deformed metagabbros (amphibolites to hornblendites) are characterised by the presence of both Mg-hornblende and plagioclase and by the development of

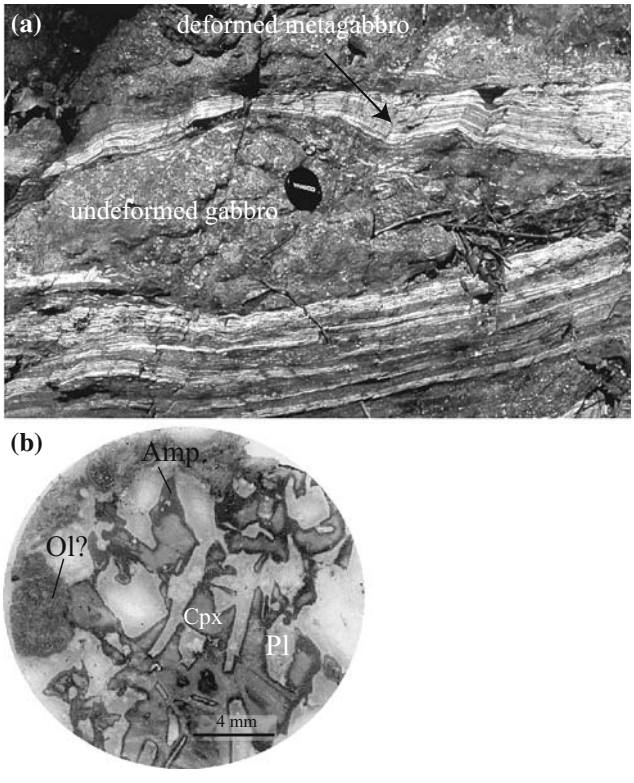

Fig. 2 **a** Boudin of undeformed gabbro in a mylonitic metagabbro. **b** Thin section of an undeformed gabbro preserving relics of igneous plagioclase and pyroxene. Clinopyroxene is invariably rimmed by green amphibole, and the round-shaped amphibole aggregates are interpreted as pseudomorphs after olivine

porphyroblastic garnet in Fe-rich protoliths; pressure and temperature values of 0.4–0.7 GPa and 500–600°C have been proposed for the amphibolite-facies metamorphic re-equilibration (Braga and Tribuzio 1999).

Eclogites

High-pressure paragenetic relics (Fig. 3) consist of euhedral garnet porphyroblasts, omphacite, zoisite, rutile, kyanite, phengite and quartz. Omphacite ($Jd_{32–41}$) is partially replaced by diopside-andesine symplectites. Garnet porphyroblasts are almandine-rich (49–62%) with lower amounts of grossular and pyrope (19–29% and 13–27%, respectively) and less than 3% spessartine; they are commonly zoned, with a decrease in Mn and Ca and a slight increase in Mg/(Mg+Fe) from core to rim (see also Messiga et al. 1992). Garnets are rimmed by green amphibole and plagioclase kelyphites. Kyanite is rimmed by fine-grained muscovite (± margarite) and quartz aggregates.

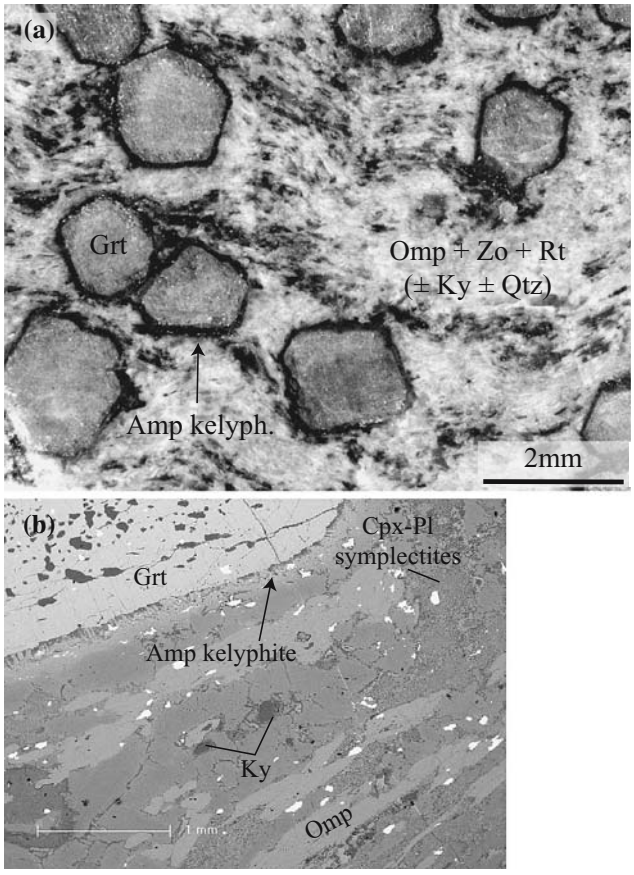

Fig. 3 **a** Photograph of a polished eclogite sample highlighting the zoned syn- to post-kinematic garnet porphyroblasts rimmed by amphibole kelyphites; the deformed matrix mainly consists of omphacite, rutile and zoisite. **b** Back-scattered electron image of an eclogite sample: the relict eclogite-facies minerals are variably overprinted by lower pressure mineral parageneses

Minimum pressure conditions of 1.7 GPa were proposed for the eclogite facies paragenesis (Cortesogno et al. 1997). Eclogite facies temperatures based on clinopyroxene-garnet Mg-Fe^{2+} exchange range from 650° to 750°C. The pressure-temperature conditions of the major late amphibolite-facies overprint are constrained to about 0.4–0.7 GPa and ~600 °C (Braga and Tribuzio 1999; Cortesogno et al. 2004).

Chemistry

Whole rock geochemistry

Selected gabbros and eclogites have significantly different major and trace element chemical compositions. At nearly constant SiO_2 contents, the gabbros have higher Al_2O_3, MgO and CaO contents and lower TiO_2, Na_2O and MnO contents than the eclogites. K_2O contents are generally low (0.1–0.9 wt%), particularly in the gabbros where they never exceed 0.2 wt%. The mg# value of the gabbros (0.77–0.80; Fig. 4a) is significantly higher than that of the eclogites (0.51–0.67). The CIPW norm indicates that gabbros are olivine normative, supporting the hypothesis that the subrounded amphibole aggregates in the gabbros are pseudomorphs after olivine. Eclogites are hypersthene-normative.

The REE pattern of the gabbros (Fig. 4b) displays depletion in LREE relative to MREE and HREE (La_N/Sm_N = 0.6 – 0.7, Yb_N contents 3–5 times those in chondrites) and a clear positive Eu anomaly (Eu/Eu* = 1.6–1.8). The gabbros have low Nb, Ta, Zr, Y, Hf and Th contents.

The eclogites are slightly depleted in LREE with respect to MREE and HREE (La_N/Sm_N = 0.64–0.82), with a small to absent negative Eu anomaly (Eu/Eu*=0.89–1.06). Total REE contents are about 15–35 times those of a chondrite. The incompatible element pattern of the eclogites is smooth, with concentrations that are typically higher than in the gabbros. No significant Sr anomaly is observed. The LREE are lightly enriched relative to Th, Nb and Ta (Fig. 4b, c). U, Ba and Rb concentrations are highly variable and were not plotted in the multivariation diagrams: these elements are strongly mobile and their concentrations may have varied during the metamorphic events subsequent to the crystallisation of the igneous protolith. Present-day $^{143}Nd/^{144}Nd$ vary from 0.512965 to 0.513160 in the gabbroic rocks and from 0.513004 to 0.513129 in the eclogites; $^{147}Sm/^{144}Nd$ span from 0.193 to 0.241, thus yielding $\varepsilon Nd_{(0)}$ in the range +6.4 to +10.2.

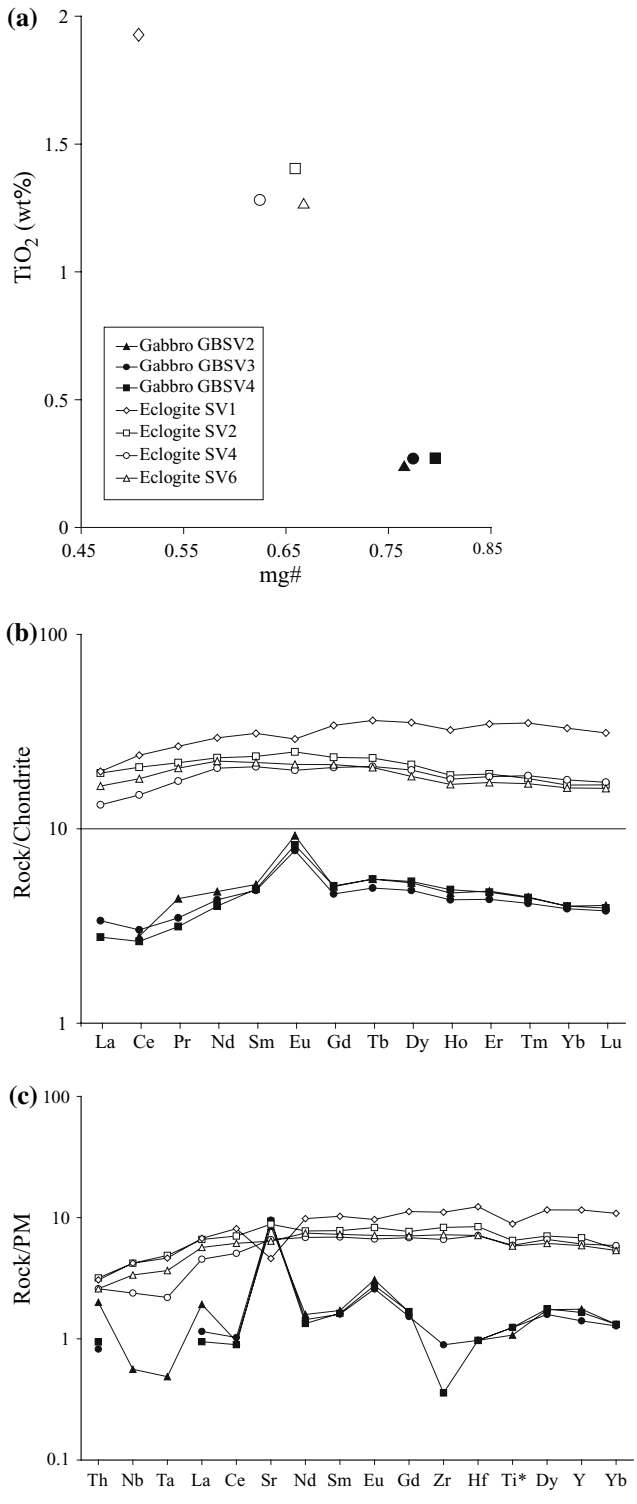

Fig. 4 **a** TiO_2 vs. mg# plot evidencing the cumulus character of the gabbroic rocks. **b** Chondrite-normalised REE diagram and **c** trace element multivariation diagram (normalised to Primitive-Mantle values) of the investigated gabbros and eclogites. Ti* is recalculated from the TiO_2 wt% in the major element analyses

Trace element composition of igneous clinopyroxene from the gabbros

The REE patterns of clinopyroxenes are characterised by LREE-depletion with respect to MREE and HREE (La_N/Sm_N = 0.07–0.17, for HREE contents 5–11 times those in chondrites) and by a weak negative Eu anomaly (Eu/Eu* = 0.7–0.9). The La_N/Sm_N ratio and the negative Eu anomaly slightly increase with total REE contents (Fig. 5; Table 3). Cr contents are relatively high (540–2600 ppm). Cr shows a rough positive correlation with mg# values. V and Sc range from 400 to 460 and from 130 to 160 ppm, respectively. The incompatible trace element patterns of the clinopyroxene (normalised to chondrite values, not reported) are characterised by low Nb, Ta, Sr, Zr and Hf contents with respect to the neighbouring REE. A remarkably similar incompatible element fingerprint is observed for clinopyroxenes from MOR-type cumulates (e.g. Tribuzio et al. 1999, 2004).

Geochronology

Zircon features

U-Pb LA-ICPMS dating of zircons was carried out on one gabbro (sample GBSV1) and one eclogite (sample SV1) from the Savona Crystalline Massif. Back-scattered electron and cathodoluminescence image analysis was completed prior to laser ablation analysis to investigate zircon morphology and internal zoning. Selected cathodoluminescence images of zircons from the two dated samples are reported in Fig. 6.

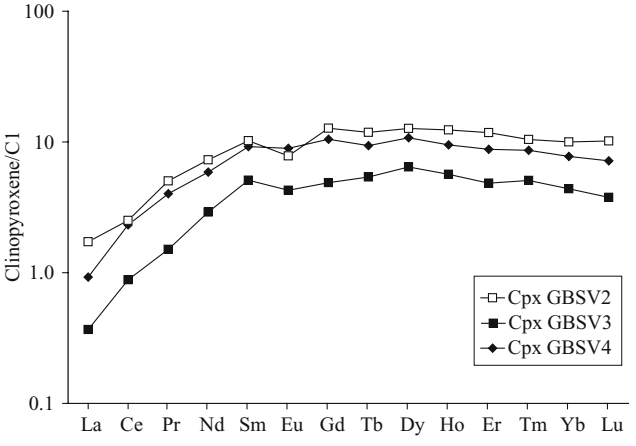

Fig. 5 Chondrite-normalised REE diagram of clinopyroxenes from the investigated gabbro samples

Table 3 Average major and trace element compositions of relict magmatic clinopyroxene from the gabbrocic rocks

Major elements (wt%)	GBSV2	GBSV4	GBSV3	Trace elements (ppm)	GBSV2	GBSV4	GBSV3
SiO_2	52.57	54.02	54.29	Sc	159	136	130
TiO_2	0.60	0.46	0.48	Ti	5037	4428	4090
Al_2O_3	2.35	2.72	2.96	V	461	400	391
Cr_2O_3	0.09	0.31	0.56	Cr	539	2386	2592
FeO	5.86	3.58	3.22	Rb	<D.L.	<D.L.	<D.L.
MnO	0.22	0.08	0.11	Sr	13.5	14.5	15.0
MgO	14.37	15.10	15.50	Y	17.5	7.88	13.1
CaO	24.27	22.80	22.76	Zr	13.8	9.89	11.3
Na_2O	0.43	1.20	1.79	Nb	0.05	0.05	0.04
Sum	100.75	100.26	101.67	Ba	<D.L.	<D.L.	<D.L.
				La	0.40	0.09	0.22
mg#	0.81	0.88	0.90	Ce	1.52	0.53	1.40
				Pr	0.45	0.13	0.36
a.p.f.u.				Nd	3.30	1.31	2.66
Si	1.93	1.96	1.93	Sm	1.50	0.75	1.36
Ti	0.02	0.01	0.01	Eu	0.44	0.24	0.50
Al	0.10	0.12	0.12	Gd	2.50	0.96	2.06
Cr	0.00	0.01	0.02	Tb	0.43	0.20	0.34
Fe^{2+}	0.14	0.10	0.01	Dy	3.08	1.56	2.62
Fe^{3+}	0.04	0.01	0.09	Ho	0.69	0.32	0.53
Mn	0.01	0.00	0.00	Er	1.87	0.77	1.39
Ni	0.00	0.00	0.00	Tm	0.25	0.12	0.21
Mg	0.78	0.82	0.82	Yb	1.62	0.71	1.26
Ca	0.95	0.89	0.87	Lu	0.25	0.09	0.17
Na	0.03	0.08	0.12	Hf	0.79	0.72	0.63
Sum	4.00	4.00	4.00	Ta	0.01	0.04	0.03

mg# : molar Mgo/(MgO+FeO)

<*D.L.* below detection limits

Zircons from the gabbro are rare and small, not exceeding 100 microns in length. Back-scattered imaging revealed that almost all zircons are short prismatic, subhedral to euhedral. A few subrounded grains also occur. The cathodoluminescence is generally low: some zircons appear nearly structureless with faint convolute zoning, while others show well developed oscillatory zoning.

Zircons in eclogites are 50–150 microns in length and show subhedral, short prismatic to anhedral and subrounded morphologies. Quartz, apatite and subordinate zoisite inclusions occur in some grains. One fractured zircon rim hosts two small inclusions of clinopyroxene-plagioclase symplectites (Fig. 6). Cathodoluminescence analysis reveals a variety of internal structures. Zircons with internal patchy zoning and strong luminescence contrasts are frequent. Several grains have cores with low luminescence and bright rims. The dark cores may be zoned (patchy or oscillatory) or almost structureless. The bright rims are unzoned.

Geochronological results

The U/Pb isotope compositions of zircons are reported in Tables 4 and 5.

Twenty-two laser ablation spots were made on sixteen zircon grains from gabbro GBSV1. Eleven ages are concordant and span a time interval from 2,136 to 459 Ma (Fig. 7). Six concordant analyses, obtained from subhedral, short prismatic zircons with faint oscillatory zoning have ages of 481–459 Ma with a mean concordant age of 469 ± 6 Ma (MSWD = 0.6, probability = 0.5). Three grains have slightly older ages ranging from 494 to 515 Ma. They have variable internal structures, with complex convolute zoning or dark unzoned areas. One subhedral, rounded crystal has a concordant age of 2,128 Ma (average of 2 analytical spots). It shows sector zoning and alternating bright and dark areas. The other analyses yield discordant points and do not define reliable intercept ages.

Eighty-three laser ablation spots on fifty-nine grains were performed on zircons from the selected eclogite. Fifty-one analyses gave concordant ages with a wide scatter of 645–305 Ma (Fig. 8a). The generally complex

Fig. 6 Cathodoluminescence images of representative zircons ▶ from the gabbro (1–5) and eclogite (6–13) and location of geochronological and microchemical analyses (Tables 4, 5, 6). Images 13 and 14 are respectively CL and BSE images of the same grain: note the inclusion of clinopyroxene-plagioclase symplectite and the thin fractures in the host zircon

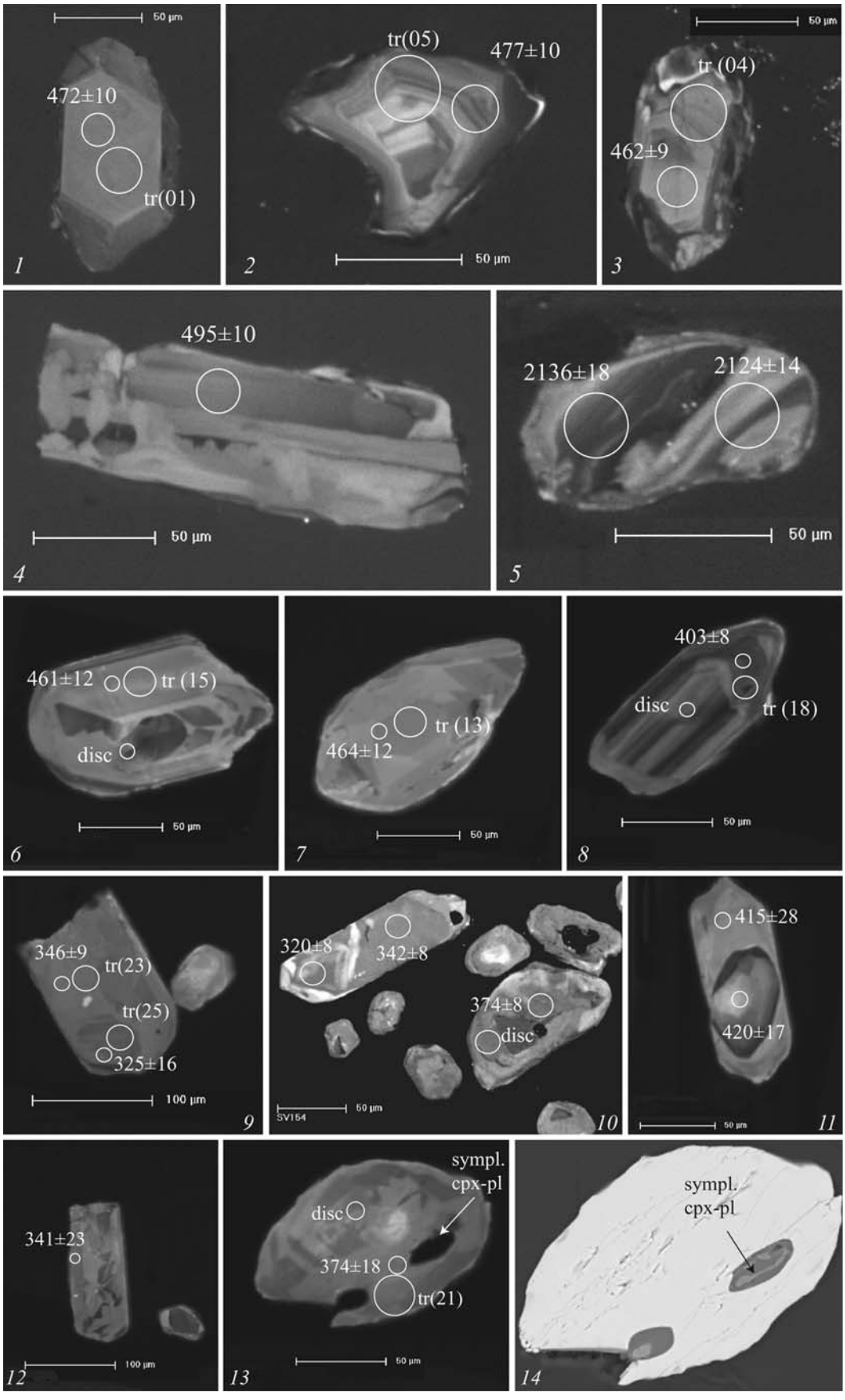
50 µm
472±10
tr(01)
1
tr(05)
477±10
50 µm
2
50 µm
tr (04)
462±9
3
495±10
50 µm
4
2136±18
2124±14
50 µm
5
461±12
tr (15)
disc
50 µm
6
464±12
tr (13)
50 µm
7
403±8
disc
tr (18)
50 µm
8
346±9
tr(23)
tr(25)
325±16
100 µm
9
320±8
342±8
374±8
disc
50 µm
SV154
10
415±28
420±17
50 µm
11
341±23
100 µm
12
sympl.
cpx-pl
disc
374±18
tr(21)
50 µm
13
sympl.
cpx-pl
14

relationships between measured ages and zircon textures are summarised below.

One subhedral zircon, three dark crystal cores and one unzoned domain in a zircon fragment yielded concordant ages of 645–520 Ma. Another twenty-five analyses of core and rim portions in euhedral-subhedral, short prismatic zircon crystals yielded concordant ages of 486–430 Ma. The internal textures vary from dominant faint oscillatory or patchy zoning, to rare fir-tree zoning. This large group of data presents an irregular bell-shaped distribution centred at about 460 Ma. Due to the large scatter, the data define two mean concordant ages (Fig. 8b): the seventeen oldest analyses cluster around a well-defined mean concordant age of 468 ± 4 Ma (MSWD = 1.2, probability = 0.3), whereas the other seven define a younger mean age of 446 ± 2 (MSWD = 1.8, probability = 0.2).

Nineteen analyses on both core and rim zircon domains with variable internal textures yielded ages in the 420–305 Ma range. These crystals are generally characterised by low luminescence and have variable internal zoning: the most frequent features are dark unzoned cores surrounded by brighter unzoned rims, or irregular crystal sectors characterised by faint luminescence contrasts. Four analyses performed on one zircon core and on three overgrowths resulted in a mean concordant age of 407 ± 9 Ma (MSWD = 0.11 probability = 0.7). Seven analytical points span from 392 to 374 Ma and form two small groups (comprising 3 and 4 analyses respectively): they define two mean concordant ages of 392 ± 4 Ma (high MSWD of 3.3) and 376 ± 2 Ma (MSWD = 1.8, probability = 0.2) respectively. In particular, the unzoned and fractured zircon rim containing two ovoid inclusions of clinopyroxene-plagioclase symplectites yielded a concordant age of 374 ± 18 Ma.

Lastly, eight analyses of irregularly zoned crystals and of bright unzoned rims on older cores yielded concordant ages ranging from about 346 to 305 Ma. Excluding the single younger analysis at 305 ± 6 Ma, the seven remaining points (Fig. 8c) define a mean Concordia age of 333 ± 7 Ma (MSWD = 0.104, probability 0.75).

Zircon trace element composition: magmatic and metamorphic zircons

Five zircon crystals from the gabbro were selected for trace element analysis: the specimens display oscillatory zoning in CL images and have ages of 459–477 Ma (Fig. 9). They have high Y (550–2,000 ppm), Hf (7,700–10,000 ppm), Th (80–470 ppm) and U (180–530 ppm) concentrations, with Th/U ratios of 0.35–1.07. The C1-chondrite normalised REE pattern is characterised by strong enrichment in HREE with respect to LREE, with Ce_N/Yb_N values ranging from 0.002 to 0.1. Ce is enriched with respect to Pr and La (La concentrations are often below the detection limit) and Eu is always depleted with respect to the neighbouring REE (Eu/Eu* = 0.02–0.55). This trace element fingerprint and the oscillatory zoning in CL images indicate zircon growth under igneous conditions (Bea and Montero 1999; Schaltegger et al. 1999; Rubatto and Gebauer 2000; Rubatto 2002).

Twenty-one dated zircon grains from eclogite SV1 were also selected for trace element analysis (Fig. 10). The zircons with concordant ages of 480 to 446 Ma are characterised by relatively high Hf (8,800–12,000 ppm), Y (250–500 ppm), Th (10–53 ppm) and U (68–900 ppm) concentrations. Th/U values are higher than 0.03, whereas the chondrite-normalised REE patterns display a steady HREE enrichment with respect to LREE ($Ce_N/Yb_N < 0.003$) and a negative Eu anomaly (Eu/Eu* = 0.2–0.6). As in the case of the analysed zircons from the gabbro, this chemical fingerprint, together with their dominant subhedral shape and the internal texture of selected crystals (characterised by faint oscillatory or patchy zoning), is typical of zircons formed under igneous conditions.

The chondrite-normalised REE pattern of two zircon rims dated at 419 ± 10 Ma and 403 ± 8 Ma are similar to those of the magmatic zircons described above, with a negative Eu anomaly and HREE enrichments over MREE and LREE. However, the textures of these rims and of all analysed zircons with ages in the 420–400 Ma range are typical of metamorphic zircons: such ages were all measured in crystal overgrowths or in unzoned and badly-defined crystal sectors with generally low luminescence. The chemical features of these zircons thus partially overlap with those of the older igneous zircons, but their internal textures and the younger ages indicate solid state recrystallisation under metamorphic conditions (Hoskin and Black 2000).

The trace element composition of seven zircon sectors spanning in age from 392 to 325 Ma are characterised by low Y, Th and U contents (35–132 ppm, 0.05–7.84 ppm and 76–197 ppm, respectively) and by Th/U contents usually below 0.02. The MREE and HREE patterns are nearly flat with low concentrations that are 70–100 times typical chondrite values; LREE contents are generally below the detection limit. These chemical features, together with their complex internal texture (presence of overgrowths, irregular sector zoning) are typical of zircons grown (or possibly recrystallised) under metamorphic conditions (Schaltegger et al. 1999;

Table 4 LA-ICP-MS U-Th-Pb isotope analyses and calculated ages of zircons from gabbro GBSV1

Zircon #	Analysis #	Spot size (μm)	Isotopic ratios								Age estimates								Concordia age	
			$^{207}Pb/^{206}Pb$	rsd	$^{206}Pb/^{238}U$	rsd	$^{207}Pb/^{235}U$	rsd	$^{208}Pb/^{232}Th$	rsd	$^{207}Pb/^{206}Pb$	1σ	$^{206}Pb/^{238}U$	1σ	$^{207}Pb/^{235}U$	1σ	$^{208}Pb/^{232}Th$	1σ	Age (Ma)	2σ
zircon 1	Lu12b05	25	0.0574	1.38	0.0832	1.07	0.6592	1.39	0.0235	1.02	507	30	515	5	514	6	470	5	515	10
zircon 3a	Lu12b06	25	0.0559	1.65	0.0760	1.08	0.5860	1.64	0.0233	1.72	446	36	472	5	468	6	466	8	472	10
zircon 10b	Lu12b07	25	0.0595	1.78	0.0776	1.11	0.6356	1.77	0.0247	1.95	585	38	482	5	500	7	493	10	disc	
zircon 3b	Lu12b08	25	0.0707	1.40	0.1070	1.08	1.0428	1.41	0.0340	1.06	949	28	655	7	725	7	675	7	disc	
zircon 10a	Lu12b09	25	0.0928	1.29	0.0833	1.08	1.0653	1.31	0.0311	0.97	1483	24	516	5	736	7	619	6	disc	
zircon 9b	Lu12b10	25	0.0720	1.58	0.0777	1.09	0.7705	1.58	0.0277	1.12	985	32	482	5	580	7	553	6	disc	
zircon 20a	Lu12b11	25	0.0939	1.18	0.0874	1.06	1.1323	1.21	0.0347	0.92	1506	22	540	6	769	7	690	6	disc	
zircon 7	Lu12b12	25	0.0571	1.94	0.0767	1.08	0.6045	1.90	0.0230	1.52	496	42	476	5	480	7	460	7	477	10
zircon 24	Lu12b13	25	0.0563	1.85	0.0760	1.08	0.5897	1.81	0.0234	1.67	463	41	472	5	471	7	467	8	472	10
zircon 9a	Lu12b14	25	0.0570	1.37	0.0796	1.03	0.6266	1.35	0.0239	1.00	493	30	494	5	494	5	478	5	494	10
zircon 11	Lu12b15	25	0.0565	1.24	0.0742	1.02	0.5780	1.24	0.0304	1.61	470	27	462	5	463	5	605	10	462	9
zircon 16	Lu12b16	25	0.0641	1.25	0.0749	1.04	0.6625	1.26	0.0250	1.04	745	26	466	5	516	5	498	5	disc	
zircon 12	Lu12b17	25	0.1907	1.11	0.0872	1.05	2.2944	1.12	0.0970	0.88	2748	18	539	5	1211	8	1870	16	disc	
zircon 4	Lu12b18	25	0.0619	1.61	0.0827	1.06	0.7064	1.60	0.0264	1.10	671	34	512	5	543	7	526	6	disc	
zircon 20b	Lu12b19	25	0.0575	1.63	0.0797	1.07	0.6330	1.62	0.0254	1.10	512	36	495	5	498	6	506	5	495	10
zircon 31	Lu12b22	25	0.0567	1.18	0.0734	1.05	0.5745	1.21	0.0212	0.89	480	26	457	5	461	4	425	4	459	9
zircon 25a	Lu12b23	25	0.1319	1.11	0.3905	1.05	7.1063	1.13	0.1087	1.02	2123	19	2125	19	2125	10	2085	20	2124	14
zircon 25b	Lu12b24	25	0.1331	1.19	0.3878	1.10	7.1293	1.25	0.1188	1.17	2140	21	2113	20	2128	11	2268	25	2136	18
zircon 6	Lu12b25	25	0.0705	1.49	0.0987	1.11	0.9595	1.52	0.0355	1.24	943	30	607	6	683	8	706	9	disc	
zircon 13	Lu12b26	25	0.0631	2.87	0.0753	1.26	0.6559	2.84	0.0259	2.20	711	60	468	6	512	11	517	11	disc	
zircon 29	Lu12b27	25	0.0688	3.90	0.0660	1.41	0.6258	3.79	0.0202	2.58	892	78	412	6	494	15	404	10	disc	
zircon 10c	Lu12b28	25	0.0573	2.78	0.0775	1.20	0.6113	2.73	0.0246	1.87	501	61	481	6	484	11	490	9	481	11

disc discordant

Table 5 LA-ICP-MS U-Th-Pb isotype analyses and calculated ages of zircons from eclogite SV1

Zircon #	Analysis #	Spot size (μm)	Isotopic ratios								Age estimates								Concordia age	
			$^{207}Pb/^{206}Pb$	rsd	$^{206}Pb/^{238}U$	rsd	$^{207}Pb/^{235}U$	rsd	$^{208}Pb/^{232}Th$	rsd	$^{207}Pb/^{206}Pb$	1σ	$^{206}Pb/^{238}U$	1σ	$^{207}Pb/^{235}U$	1σ	$^{208}Pb/^{232}Th$	1σ	Age (Ma)	2σ
SV1_4-1a-R	Ap05c05	10	0.0737	5.64	0.0585	1.83	0.5908	5.50	NA	–	1034	110	366	7	471	21	–	–	disc	
SV1_4-1b-C	Ap05c06	10	0.0577	2.74	0.0741	1.32	0.5825	2.73	NA	–	518	59	461	6	466	10	–	–	461	12
SV1_-3C	Ap05c07	10	0.0605	3.54	0.0745	1.30	0.6170	3.47	NA	–	622	75	463	6	488	13	–	–	464	12
SV1_4-5-C	Ap05c08	10	0.0578	3.32	0.0866	1.40	0.6854	3.29	NA	–	522	72	535	7	530	14	–	–	535	14
SV1_4-6-C	Ap05c09	10	0.0570	3.79	0.0773	1.46	0.6029	3.75	NA	–	489	82	480	7	479	14	–	–	480	13
SV1_4-7a-R	Ap05c10	10	0.0561	1.80	0.0643	1.01	0.4990	1.74	NA	–	457	39	402	4	411	6	–	–	403	8
SV1_4-7b-R	Ap05c11	10	0.0576	2.10	0.0693	1.20	0.5514	2.10	NA	–	513	46	432	5	446	8	–	–	disc	
SV1_4-8a	Ap05c12	10	0.0554	6.20	0.0710	1.75	0.5437	6.09	NA	–	427	133	442	7	441	22	–	–	442	15
SV1_4-8b	Ap05c13	10	0.0610	4.49	0.0720	1.53	0.6081	4.41	NA	–	640	94	448	7	482	17	–	–	disc	
SV1_4-9	Ap05c14	10	0.0586	3.26	0.0759	1.16	0.6144	3.17	NA	–	551	70	472	5	486	12	–	–	472	11
SV1_4-10	Ap05c18	10	0.0562	5.06	0.0720	1.43	0.5593	4.97	NA	–	458	109	448	6	451	18	–	–	448	12
SV1_4-12a	Ap05c19	10	0.0604	3.57	0.0761	1.42	0.6261	3.51	NA	–	619	75	473	6	494	14	–	–	473	13
SV1_4-12b	Ap05c20	10	0.0565	5.05	0.0735	1.52	0.5768	4.95	NA	–	471	109	457	7	462	18	–	–	458	13
SV1_3-11	Ap05c21	10	0.0898	4.84	0.0707	1.60	0.8757	4.70	NA	–	1421	90	441	7	639	22	–	–	disc	
SV1_3-9a	Ap05c22	10	0.0527	5.55	0.0551	1.47	0.4002	5.46	NA	–	314	121	346	5	342	16	–	–	346	9
SV1_3-9b	Ap05c23	10	0.0577	10.82	0.0517	2.50	0.4064	10.58	NA	–	517	222	325	8	346	31	–	–	325	16
SV1_3-8	Ap05c24	10	0.0414	10.08	0.0742	1.63	0.4263	10.00	NA	–	–	–	462	7	361	30	–	–	disc	
SV1_3-7a	Ap05c25	10	0.0565	5.37	0.0716	1.48	0.5591	5.27	NA	–	470	115	446	6	451	19	–	–	446	13
SV1_3-7b	Ap05c26	10	0.0566	7.50	0.0840	1.81	0.6573	7.36	NA	–	474	158	520	9	513	30	–	–	520	18
SV1_3-5b	Ap05d05	10	0.0559	4.21	0.0690	1.29	0.5278	4.11	NA	–	446	91	430	5	430	14	–	–	430	11
SV1_2-1	Ap05d06	10	0.0560	23.93	0.0720	4.21	0.5566	23.62	NA	–	454	458	448	18	449	86	–	–	448	36
SV1_2-2	Ap05d07	10	0.1011	12.39	0.0806	3.52	1.1215	11.99	NA	–	1645	214	500	17	764	64	–	–	disc	
SV1_2-6-C	Ap05d09	10	0.0551	8.42	0.0673	2.10	0.5109	8.26	NA	–	416	178	420	9	419	28	–	–	420	17
SV1_2-9	Ap05d13	10	0.0374	25.08	0.1060	3.28	0.5493	24.91	NA	–	–	–	649	20	445	90	–	–	disc	
SV1_1-5a-C	Ap05d16	10	0.0558	2.97	0.0849	1.32	0.6555	2.93	NA	–	446	65	525	7	512	12	–	–	524	13
SV1_1-5b-R	Ap05d17	10	0.0573	8.13	0.0536	1.70	0.4267	8.00	NA	–	504	170	337	6	361	24	–	–	337	11
SV1_1-4-R	Ap05d18	10	0.0529	16.34	0.0597	2.45	0.4385	16.20	NA	–	326	334	374	9	369	50	–	–	374	18
SV1_1-4-C	Ap05d19	10	0.0179	20.94	0.0778	2.38	0.1934	20.83	NA	–	–	–	483	11	180	34	–	–	disc	
SV1_4-5-R	Ap05d21	10	0.0548	1.64	0.0794	1.03	0.6057	1.61	NA	–	403	36	493	5	481	6	–	–	disc	
SV1_1a-C	Lu13b08	25	0.0540	3.15	0.0545	1.17	0.4059	3.07	0.0340	1.06	949	28	655	7	725	7	675	7	342	8
SV1_1b-R	Lu13b09	25	0.0532	3.29	0.0508	1.24	0.3742	3.20	0.0311	0.97	1483	24	516	5	736	7	619	6	320	8
SV1_2a-C	Lu13b10	25	0.0561	2.76	0.0597	1.07	0.4617	2.67	0.0277	1.12	985	32	482	5	580	7	553	6	374	8
SV1_2b-R	Lu13b11	25	0.0641	3.85	0.0592	1.27	0.5242	3.74	0.0347	0.92	1506	22	540	6	769	7	690	6	disc	
SV1_3-C	Lu13b12	25	0.0582	1.91	0.0508	0.91	0.4079	1.79	0.0230	1.52	496	42	476	5	480	7	460	7	disc	
SV1_4a-R	Lu13b13	25	0.0578	3.19	0.0756	1.08	0.6027	3.08	0.0234	1.67	463	41	472	5	471	7	467	8	470	10
SV1_4b-R	Lu13b14	25	0.0653	2.79	0.0692	1.05	0.6240	2.67	0.0239	1.00	493	30	494	5	494	5	478	5	disc	
SV1_5a-R	Lu13b15	25	0.0559	1.77	0.0626	0.89	0.4823	1.66	0.0236	3.52	446	39	391	3	400	5	471	16	392	8
SV1_5b-R	Lu13b16	25	0.0664	3.21	0.0471	1.21	0.4321	3.10	0.0250	1.04	745	26	466	5	516	5	498	5	disc	
SV1_6a-C	Lu13b17	25	0.0516	3.93	0.0523	1.26	0.3727	3.83	0.0970	0.88	2748	18	539	5	1211	8	1870	16	328	8
SV1_6b-R	Lu13b18	25	0.0520	2.14	0.0485	1.03	0.3470	2.07	0.0264	1.10	671	34	512	5	543	7	526	6	305	6
SV1_7a-C	Lu13b21	25	0.0561	1.07	0.0825	0.84	0.6381	0.93	0.0150	1.47	581	47	315	3	349	6	300	4	disc	

Table 5 continued

Zircon #	Analysis #	Spot size (μm)	Isotopic ratios								Age estimates								Concordia age	
			$^{207}Pb/^{206}Pb$	rsd	$^{206}Pb/^{238}U$	rsd	$^{207}Pb/^{235}U$	rsd	$^{208}Pb/^{232}Th$	rsd	$^{207}Pb/^{206}Pb$	1σ	$^{206}Pb/^{238}U$	1σ	$^{207}Pb/^{235}U$	1σ	$^{208}Pb/^{232}Th$	1σ	Age (Ma)	2σ
SV1_7b-R	Lu13b22	25	0.0556	1.15	0.0773	0.84	0.5927	1.02	0.0212	0.89	480	26	457	5	461	4	425	4	disc	
SV1_6c R	Lu13b23	25	0.0695	2.32	0.0545	0.95	0.5226	2.19	0.1087	1.02	2123	19	2125	19	2125	10	2085	20	disc	
SV1_8a-R	Lu13b24	25	0.0594	2.91	0.0551	1.03	0.4516	2.78	0.1188	1.17	2140	21	2113	20	2128	11	2268	25	disc	
SV1_8b-C	Lu13b25	25	0.0618	3.13	0.0532	1.05	0.4526	3.01	0.0355	1.24	943	30	607	6	683	8	706	9	disc	
SV1_9a-C	Lu13b26	25	0.0625	1.90	0.0741	0.89	0.6385	1.78	0.0259	2.20	711	60	468	6	512	11	517	11	disc	
SV1_10a-C	Lu13b27	25	0.0587	2.16	0.0901	0.92	0.7293	2.04	0.0202	2.58	892	78	412	6	494	15	404	10	556	10
SV1_10b-R	Lu13b28	25	0.0570	1.61	0.0728	0.85	0.5724	1.48	0.0246	1.87	501	61	481	6	484	11	490	9	454	7
SV1_11a-R	Lu13b29	25	0.0809	4.50	0.0502	1.50	0.5597	4.34	0.0170	0.88	360	24	371	4	370	3	341	3	disc	
SV1_11b-R	Lu13b30	25	0.1178	2.60	0.0569	1.20	0.9248	2.45	0.0151	0.86	377	23	287	3	297	3	303	3	disc	
SV1_12-C	Lu13b31	25	0.0655	4.15	0.0749	1.35	0.6771	4.02	0.0121	0.82	511	23	292	3	318	3	244	2	disc	
SV1_13-C	Lu13b32	25	0.0567	7.41	0.0778	1.88	0.6079	7.25	0.0182	0.88	390	27	353	4	358	4	365	3	483	17
SV1_14- C	Lu13b33	25	0.0539	3.92	0.0597	1.16	0.4430	3.79	0.0098	0.82	518	22	243	2	270	2	196	2	374	8
SV1_15a-C	Lu13b34	25	0.0735	3.67	0.0759	1.34	0.7600	3.56	0.0162	0.80	578	23	302	3	336	3	325	3	disc	
SV1_15b-R	Lu13b35	25	0.0524	3.80	0.0673	1.25	0.4806	3.70	0.1027	1.25	2958	27	295	3	889	10	1976	23	419	10
SV1_16-C	Lu13b36	25	0.0560	5.07	0.0742	1.50	0.5652	4.95	0.0194	0.88	379	24	365	4	367	3	389	3	461	13
SV1-17-C	Lu13c05	25	0.0577	1.32	0.0756	0.95	0.6012	1.25	0.0240	1.04	519	29	470	4	478	5	479	5	disc	
SV1-18-C	Lu13c06	25	0.0780	1.82	0.0777	1.06	0.8349	1.76	0.0447	1.72	1146	36	482	5	616	8	884	15	disc	
SV1-19-R	Lu13c07	25	0.0683	2.59	0.0556	1.15	0.5235	2.51	0.2054	9.14	878	53	349	4	428	9	3776	315	disc	
SV1-20-C	Lu13c08	25	0.0635	1.87	0.0838	1.05	0.7333	1.82	0.0363	2.12	724	39	519	5	559	8	721	15	disc	
SV1-21-C	Lu13c09	25	0.0557	2.05	0.0741	1.07	0.5685	1.99	0.0255	2.27	439	45	461	5	457	7	510	11	460	9
SV1-22-C	Lu13c10	25	0.0579	1.87	0.0762	1.06	0.6083	1.81	0.0255	1.57	525	41	474	5	483	7	509	8	474	10
SV1-23-R	Lu13c11	25	0.0564	1.56	0.0735	1.03	0.5715	1.53	0.0232	1.25	467	35	457	5	459	6	463	6	458	9
SV1-23-C	Lu13c12	25	0.0560	1.52	0.0726	1.03	0.5610	1.48	0.0240	1.21	454	33	452	4	452	5	479	6	452	9
SV1-24-C	Lu13c13	25	0.0603	1.58	0.0712	1.00	0.5917	1.52	0.0267	1.61	613	34	444	4	472	6	533	8	disc	
SV1-25-C	Lu13c14	25	0.0566	1.78	0.0761	1.01	0.5937	1.72	0.0278	1.77	475	39	473	5	473	7	553	10	473	9
SV1-26-R	Lu13c22	25	0.0546	1.19	0.0645	1.07	0.4859	1.22	0.0180	1.68	396	26	403	4	402	4	360	3	402	8
SV1-27-R	Lu13c28	25	0.0565	1.45	0.0785	1.03	0.6095	1.43	0.0259	1.04	471	32	487	5	483	5	518	5	486	9
Sv1-28-C	Ma29b16	25	0.0551	1.72	0.0734	1.06	0.5613	1.70	0.0219	2.97	417	38	457	5	452	6	438	13	456	9
SV1-29-C	Ma29b17	25	0.0568	1.32	0.0790	0.90	0.6184	1.22	0.0265	1.13	483	29	490	4	489	5	528	6	490	8
SV1-30-R	Ma29b18	25	0.0549	1.86	0.0605	0.93	0.4574	1.75	0.0236	2.25	408	41	379	3	383	6	470	11	379	7
SV1-31-C	Ma29b23	25	0.0568	1.83	0.0756	0.93	0.5911	1.73	0.0206	1.55	484	40	470	4	472	7	413	6	470	8
SV1-32-C	Ma29b24	25	0.0564	2.52	0.0707	1.00	0.5493	2.41	0.0290	2.69	468	55	441	4	445	9	579	15	441	8
SV1-33-C	Ma29b25	25	0.0549	2.26	0.0627	0.96	0.4740	2.14	0.0095	4.20	408	49	393	4	391	7	192	8	392	7
SV1-33-R	Ma29b26	25	0.0437	1.83	0.0620	0.87	0.3724	1.72	0.0214	1.31	–	–	388	3	321	5	428	6	disc	
SV1-34-C	Ma29b27	25	0.0638	1.49	0.0727	0.88	0.6379	1.36	0.0277	1.34	733	31	452	4	501	5	552	7	disc	
SV1-35-C	Ma29b28	25	0.0579	1.95	0.0796	0.93	0.6343	1.84	0.0291	2.30	526	42	494	4	499	7	580	13	494	9
SV1-36-C	Ma29b29	25	0.0623	12.87	0.1052	3.44	0.9030	12.59	0.0960	19.34	686	253	645	21	653	61	1854	343	645	42
SV1-37-R	Ma29b30	25	0.0556	2.70	0.0627	1.04	0.4800	2.59	–	–	436	59	392	4	398	9	–	–	392	8
SV1-38-C	Ma29b31	25	0.0570	1.56	0.0745	0.98	0.5854	1.49	0.0225	1.51	493	34	463	4	468	6	449	7	464	9
SV1-39-C	Ma29b32	25	0.0518	1.00	0.0787	0.91	0.5604	0.93	0.0225	1.11	276	23	489	4	452	3	450	5	disc	
SV1-39-R	Ma29b33	25	0.0550	1.05	0.0698	0.92	0.5274	0.97	0.0209	1.15	412	23	435	4	430	3	417	5	disc	

disc discordant, NA: not analysed

Table 6 Trace element compositions of selected zircons

	Gabbro GBSV1				
Analysis	1	2	3	4	5
Location	Core	Core	Core	Core	Core
Zoning	Unzoned	Unzoned	Oscillatory	Faint oscillatory	Oscillatory
U/Pb Age (Ma)[a]	472 ± 10	459 ± 9	481 ± 11	462 ± 9	477 ± 10
Element (ppm)					
Li	3.78	1.93	5.58	3.56	2.51
Mg	2.8	10.44	1.75	20.75	2.73
Sc	201	330	156	219	198
Ti	11.55	22.91	9.76	23.27	<D.L.
V	0.51	0.75	1.48	0.59	<D.L.
Cr	<D.L.	<D.L.	<D.L.	<D.L.	<D.L.
Rb	0.22	0.51	0.37	<D.L.	<D.L.
Sr	0.27	0.33	0.11	0.11	0.22
Y	973	1811	1933	710	558
Nb	6.34	4.45	6.42	3.83	6.12
Cs	<D.L.	0.057	<D.L.	0.072	<D.L.
Ba	<D.L.	<D.L.	<D.L.	<D.L.	<D.L.
La	<D.L.	<D.L.	0.06	<D.L.	<D.L.
Ce	11.38	4.54	19.01	2.23	8.96
Pr	0.463	0.182	0.366	0.07	<D.L.
Nd	2.26	3.13	6.9	0.9	0.64
Sm	3.07	5.57	10.36	3.7	2.26
Eu	1.24	0.377	0.17	0.84	0.84
Gd	19.86	39.03	59.49	15.25	7.72
Tb	8.39	14.38	18.04	4.86	3.74
Dy	94.85	166.18	213.54	60.91	49.25
Ho	33.5	62.11	72.29	22.52	20.32
Er	147.7	267.3	293.6	100.5	92.9
Tm	34.7	57.4	61.6	22.5	18.7
Yb	379.5	550.4	512.8	208.8	183.2
Lu	59.12	93.69	84.42	38.10	35.20
Hf	8153	9674	9689	7680	9980
Ta	1.23	0.564	1.26	0.333	1.39
Pb	5.56	5.47	38.15	22.03	3.21
Th	118	100	256	467	81
U	197	286	240	528	176
Th/U	0.6017	0.3479	1.0679	0.8853	0.4584
Eu/Eu*	0.363	0.057	0.016	0.292	0.549
Ce_N/Yb_N	0.0081	0.0022	0.0100	0.0029	0.0132

Eclogite SV1										
Analysis	6	7	8	9	10	11	12	13	14	15
Location	Core	Core	Undefined	Rim	Core	Core	Core	Core	Core	Core
zoning	Dark unzoned		Unzoned bright	Bright	Patchy	Oscillatory	Patchy	Patchy	Unzoned	Faint oscillatory
U/Pb Age (Ma)[a]	535 ± 14	524 ± 13	520 ± 18	subconc. 488	480 ± 10	474 ± 10	473 ± 9	464 ± 12	464 ± 9	461 ± 12
Element (ppm)										
Li	<D.L.	<D.L.	<D.L.	<D.L.	<D.L.	<D.L.	<D.L.	<D.L.	7.84	<D.L.
Mg	<D.L.	<D.L.	160.97	<D.L.	<D.L.	<D.L.	<D.L.	<D.L.	<D.L.	<D.L.
Sc	529	545	516	542	482	415	443	463	430.21	464
Ti	<D.L.	<D.L.	38.28	<D.L.	6.91	<D.L.	<D.L.	<D.L.	2.63	<D.L.
V	1.83	<D.L.	<D.L.	1.56	1.16	0.72	<D.L.	<D.L.	0.112	<D.L.
Cr	<D.L.	<D.L.	<D.L.	21.68	<D.L.	<D.L.	15.93	<D.L.	<D.L.	33.65
Rb	<D.L.	<D.L.	<D.L.	<D.L.	3.53	<D.L.	<D.L.	<D.L.	<D.L.	<D.L.
Sr	<D.L.	<D.L.	1.16	<D.L.	0.82	<D.L.	<D.L.	<D.L.	0.226	<D.L.
Y	314	442	51	342	397	301	447	361	253.21	338
Nb	1.69	2.13	<D.L.	2.33	0.73	1.3	1.46	0.55	1.077	1.52

Table 6 continued

Eclogite SV1										
Analysis	6	7	8	9	10	11	12	13	14	15
Location	Core	Core	Undefined	Rim	Core	Core	Core	Core	Core	Core
zoning	Dark unzoned		Unzoned bright	Bright	Patchy	Oscillatory	Patchy	Patchy	Unzoned	Faint oscillatory
U/Pb Age (Ma)[a]	535 ± 14	524 ± 13	520 ± 18	subconc. 488	480 ± 10	474 ± 10	473 ± 9	464 ± 12	464 ± 9	461 ± 12
Cs	<D.L.	<D.L.	1.29	<D.L.	<D.L.	<D.L.	<D.L.	<D.L.	<D.L.	<D.L.
Ba	<D.L.	<D.L.	<D.L.	<D.L.	1.01	<D.L.	0.86	<D.L.	0.221	<D.L.
La	<D.L.	<D.L.	0.31	0.082	0.155	<D.L.	<D.L.	0.2	<D.L.	<D.L.
Ce	0.57	1.54	0.157	2.68	0.84	0.346	0.805	1.43	0.652	<D.L.
Pr	<D.L.	0.098	0.078	0.122	<D.L.	0.033	<D.L.	<D.L.	<D.L.	<D.L.
Nd	<D.L.	0.58	1.56	0.33	<D.L.	0.25	<D.L.	<D.L.	<D.L.	<D.L.
Sm	<D.L.	0.4	1.83	<D.L.	1.31	0.51	1.3	<D.L.	0.736	<D.L.
Eu	0.39	<D.L.	0.19	0.29	0.42	0.144	0.362	0.95	0.098	0.127
Gd	2.26	8.94	6.68	3.64	3.18	2.76	6.77	5.9	2.1	4.77
Tb	1.42	2.69	1.16	1.95	2.57	1.331	2.65	2.09	0.984	1.89
Dy	22.68	27.58	4.56	20.72	26.08	17.42	34.14	26.47	16.79	21.23
Ho	11.69	13.6	1.56	12.83	12.45	9.44	13.1	12.13	7.81	10.16
Er	59.0	86.6	8.7	63.6	77.8	44.6	72.0	68.8	43.63	56.5
Tm	14.7	17.8	1.7	17.0	16.2	11.6	17.9	18.6	10.88	13.8
Yb	177.4	206.7	11.7	185.6	198.5	156.8	198.4	176.1	131.25	160.1
Lu	35.85	44.25	2.70	40.31	39.79	34.51	43.31	42.37	27	37.24
Hf	13203	15088	21323	13224	12088	9618	9188	11165	8834	9462
Ta	<D.L.	0.208	0.236	<D.L.	<D.L.	0.199	0.162	<D.L.	0.163	<D.L.
Pb	0.71	4.94	<D.L.	7	1.58	1.55	0.62	0.98	0.648	1.15
Th	21	76	1	99	29	14	9	27	13.53	28
U	663	1040	65	2282	135	441	68	171	84.22	148
Th/U	0.0316	0.0729	0.0180	0.0433	0.2121	0.0316	0.1324	0.1580	0.1607	0.1903
Eu/Eu*	–	–	0.147	–	0.606	0.296	0.300	–	0.230	–
Ce_N/Yb_N	0.0008	0.0019	0.0034	0.0037	0.0011	0.0006	0.0011	0.0021	0.0013	–

Eclogite SV1										
Analysis	16	17	18	19	20	21	22	23	24	25
Location	Undefined	Core	Rim	Rim	Rim	Rim	Core	Core	Rim	Rim
zoning	Unzoned dark	Sector zoning	Unzoned	Unzoned bright	Unzoned bright	Unzoned dark	Unzoned dark	Unzoned bright	Unzoned bright	Sector zoning
U/Pb Age (Ma)[a]	446 ± 13	419 ± 10	403 ± 8	392 ± 8	392 ± 7	374 ± 18	374 ± 8	346 ± 9	337 ± 11	325 ± 16
Element (ppm)										
Li	<D.L.	<D.L.	<D.L.	<D.L.	<D.L.	<D.L.	3.62	<D.L.	<D.L.	<D.L.
Mg	24.4	<D.L.	<D.L.	<D.L.	<D.L.	<D.L.	1.61	<D.L.	23.48	<D.L.
Si	149581	154255	149581	154255	154255	149581	154255	149581	149581	149581
Sc	461	433.09	597	517.32	430.45	517	455.18	446	483	407
Ti	18.6	13.48	<D.L.	22.53	3.69	<D.L.	<D.L.	<D.L.	<D.L.	<D.L.
V	1.19	0.124	<D.L.	0.086	0.238	<D.L.	0.308	<D.L.	<D.L.	<D.L.
Cr	<D.L.	<D.L.	<D.L.	<D.L.	<D.L.	<D.L.	<D.L.	<D.L.	19.61	10.07
Rb	<D.L.	<D.L.	<D.L.	0.35	<D.L.	<D.L.	<D.L.	<D.L.	2.86	<D.L.
Sr	<D.L.	0.378	<D.L.	0.403	0.261	<D.L.	0.275	<D.L.	<D.L.	<D.L.
Y	502	231.89	1627	59.61	85.55	132	64.39	56	95	35
Zr	455349	NA	421825	NA	NA	492491	NA	420496	468846	391496
Nb	1.42	1.152	1.47	0.97	1.029	1.07	1.259	1.2	1.93	1.37
Cs	<D.L.	<D.L.	<D.L.	<D.L.	<D.L.	<D.L.	<D.L.	<D.L.	<D.L.	<D.L.
Ba	5.29	0.756	<D.L.	0.251	0.152	<D.L.	<D.L.	<D.L.	0.92	<D.L.
La	<D.L.	<D.L.	<D.L.	0.0254	0.065	<D.L.	<D.L.	<D.L.	<D.L.	
Ce	0.95	0.54	0.41	0.333	0.608	0.549	0.394	0.356	0.105	0.197
Pr	0.324	<D.L.	<D.L.	<D.L.	<D.L.	<D.L.	<D.L.	<D.L.	<D.L.	<D.L.
Nd	<D.L.	0.136	0.24	<D.L.	0.42	<D.L.	<D.L.	<D.L.	0.21	<D.L.
Sm	1.45	0.512	<D.L.	0.947	1.13	0.56	0.9	1.46	1.16	0.74
Eu	0.53	0.111	0.145	0.919	0.816	0.66	0.726	0.665	<D.L.	0.712
Gd	6.12	2.67	11.61	6.77	4.24	12.79	6.22	7.23	6.22	4.76

Table 6 continued

Eclogite SV1										
Analysis	16	17	18	19	20	21	22	23	24	25
Location	Undefined	Core	Rim	Rim	Rim	Rim	Core	Core	Rim	Rim
zoning	Unzoned dark	Sector zoning	Unzoned	Unzoned bright	Unzoned bright	Unzoned dark	Unzoned dark	Unzoned bright	Unzoned bright	Sector zoning
U/Pb Age (Ma)[a]	446 ± 13	419 ± 10	403 ± 8	392 ± 8	392 ± 7	374 ± 18	374 ± 8	346 ± 9	337 ± 11	325 ± 16
Tb	2.74	1.059	8.07	1.222	0.767	3.06	1.069	0.964	0.94	0.761
Dy	28.7	16.14	117.12	7.75	6.94	18.3	7.04	7.6	12.96	5.17
Ho	14.13	7.21	54.36	1.712	2.69	3.59	2.039	1.82	3.65	1.056
Er	85.1	38.13	282.6	6.07	11.85	13.2	7.41	5.2	14.7	4.5
Tm	19.5	8.72	67.4	0.94	3.12	1.8	1.662	1.0	3.1	0.8
Yb	241.3	107.65	657.9	9.39	37.46	18.1	18.91	7.5	15.7	7.0
Lu	59.07	23.7	128.83	1.43	8.44	3.29	3.63	1.18	2.80	0.91
Hf	10795	7998	11693	9790	8899	12062	9573	11828	16271	11718
Ta	0.346	0.19	0.736	0.159	0.107	<D.L.	0.136	0.243	<D.L.	<D.L.
Pb	2.8	1.81	1.46	0.06	0.535	0.34	0.124	0.135	<D.L.	0.368
Th	53	19.68	32	0.191	7.84	2	1.471	0	1	0
U	902	103.46	457	194.37	196.68	157	108.42	76	143	126
Th/U	0.0589	0.1902	0.0704	0.0010	0.0399	0.0143	0.0136	0.0018	0.0069	0.0004
Eu/Eu*	0.463	0.220	–	0.810	1.000	0.344	0.690	0.511	–	0.873
Ce_N/Yb_N	0.0010	0.0013	0.0002	0.0091	0.0042	0.0078	0.0054	0.0123	0.0017	0.0073

subconc subconcordant age, *<D.L.* below limits, *NA* not analysed

[a] Trace element analyses were located near the ablation spots for U/Pb geochronology: the calculated ages are here reported for reference

Hoskin and Black 2000; Rubatto 2002). In addition, the low abundance of HREE and Y suggests the presence of garnet as a chemical buffer during zircon growth/recrystallisation (Rubatto 2002).

Discussion

Protolith age and geochemical affinity of the mafic rocks

In the gabbro, zircons with oscillatory zoning and trace element compositions typical of crystallisation under igneous conditions (high Th/U ratios, high trace element contents, negative Eu anomaly) yielded a mean concordant age of 469 ± 6 Ma. This age is interpreted as the timing of zircon crystallisation in the basic magma. The presence of zircons with ages older than the inferred crystallisation age suggests the involvement of an old (crustal?) component in the petrogenesis of the gabbro.

Zircons from the eclogite yielded very scattered ages of 556–305 Ma. Zircon grains with typical igneous textures and trace element compositions concentrate in the 486–430 Ma range. These zircons define two mean

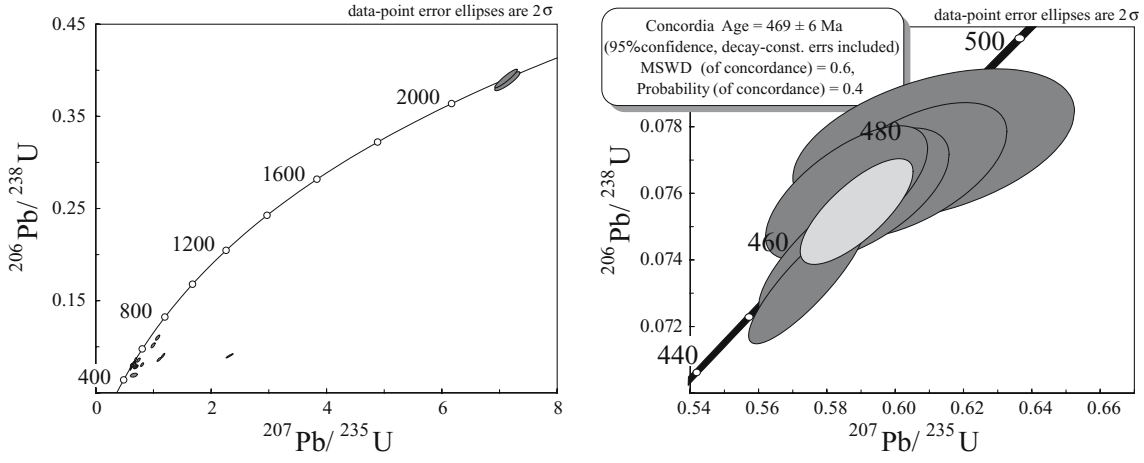

Fig. 7 U/Pb Concordia diagram (*left*) and mean Concordia age (*right*) for the analysed zircons from the gabbro

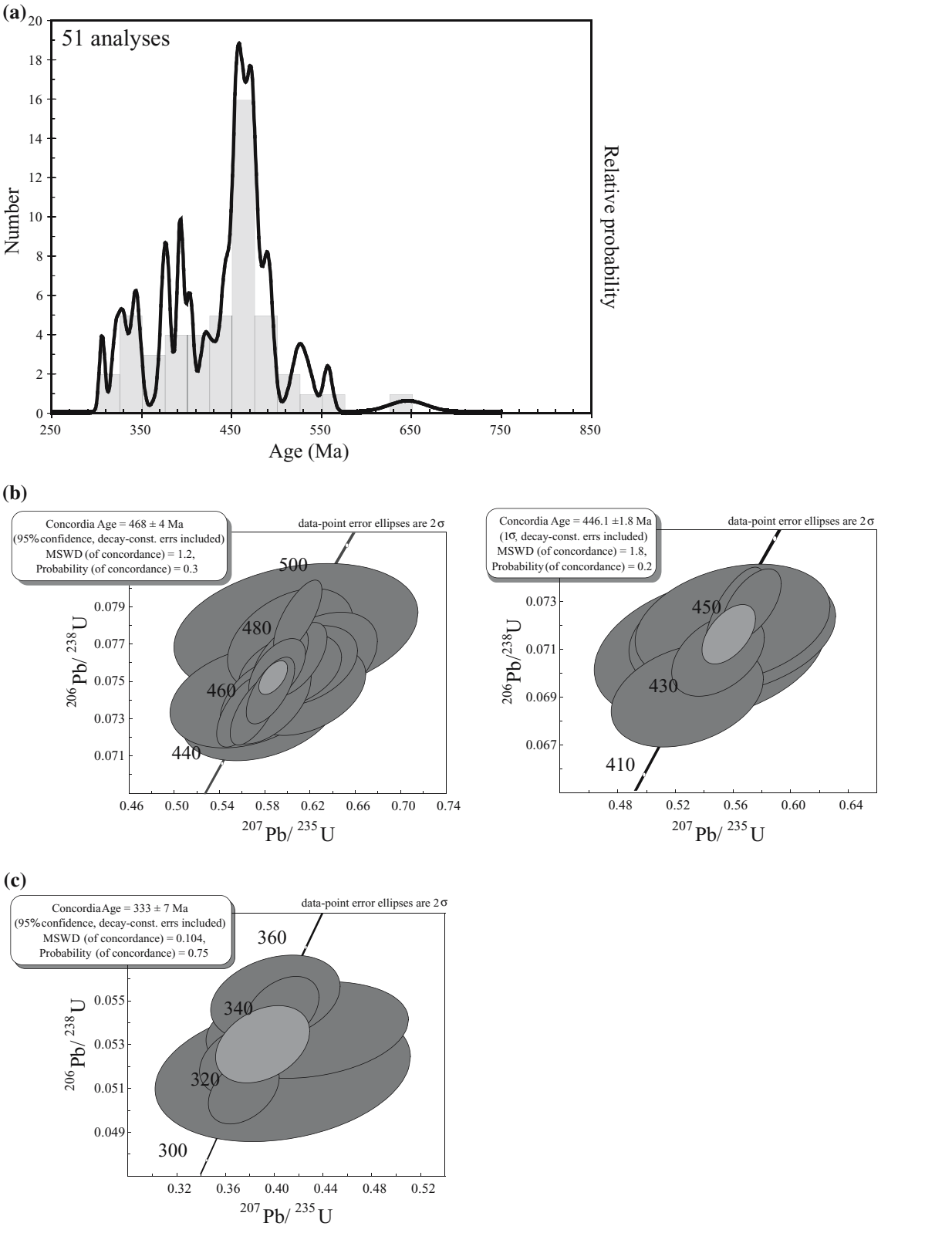

Fig. 8 **a** Density plot of the U/Pb ages for the analysed zircons from the eclogite. **b** mean Concordia ages of the oldest (igneous) zircon populations. **c** mean Concordia age of the youngest (metamorphic) zircon population. See the Discussion for further details

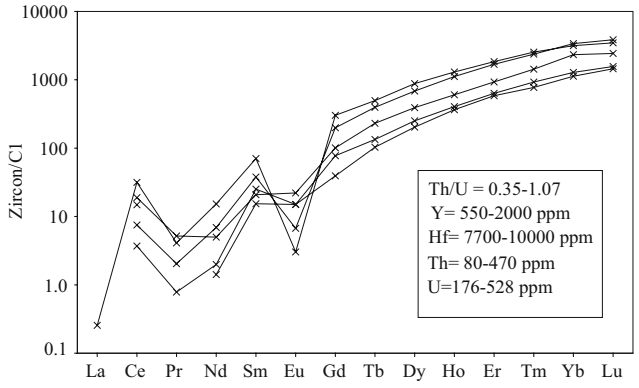

Fig. 9 REE compositions (normalised to chondrite values) of selected zircons from the gabbro

concordant ages of 468 ± 4 Ma (17 analyses, MSWD = 1.2) and 446 ± 2 Ma (7 analyses, MSWD = 1.8), respectively. This large scatter does not allow a straightforward estimate of the emplacement age for the eclogite igneous protolith.

The spread towards younger ages could result from mixed ages in relation to the textural complexity of some zircon crystals. Nevertheless, we believe that the careful observation of CL images prior to geochronological analyses and the use of small laser spots (10 μm) for the most critical zircons substantially reduced the risk of mixed analyses. The fact that the age results of analyses performed at 25 μm are comparable (within error) to those of the spatially more precise analyses performed at 10 μm, suggests that the younger zircon ages are most likely ''true'' ages and not the result of mixed analyses. In addition, the dispersion of concordant ages with igneous-like characters is often observed in magmatic rocks that underwent slow cooling rates or metamorphic re-equilibration after crystallisation (Ashwal et al. 1999; Hoskin and Black 2000; Ghezzo, personal communication). This partial

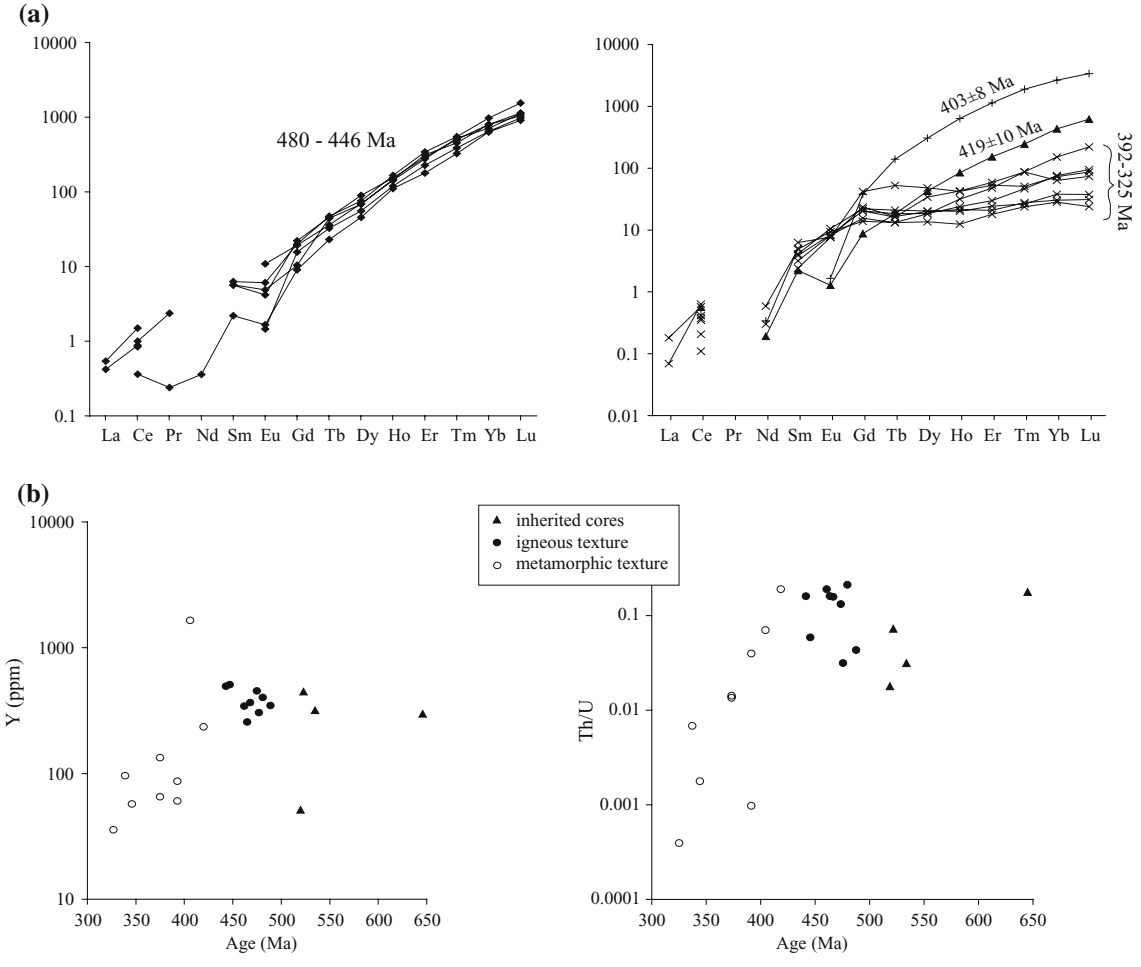

Fig. 10 **a** REE compositions (normalised to chondrite) of selected zircons from the eclogite: domains with igneous texture are on the *left*, those with metamorphic texture are on the *right*. **b** Y contents and Th/U ratio plotted against U/Pb ages of texturally different zircon domains

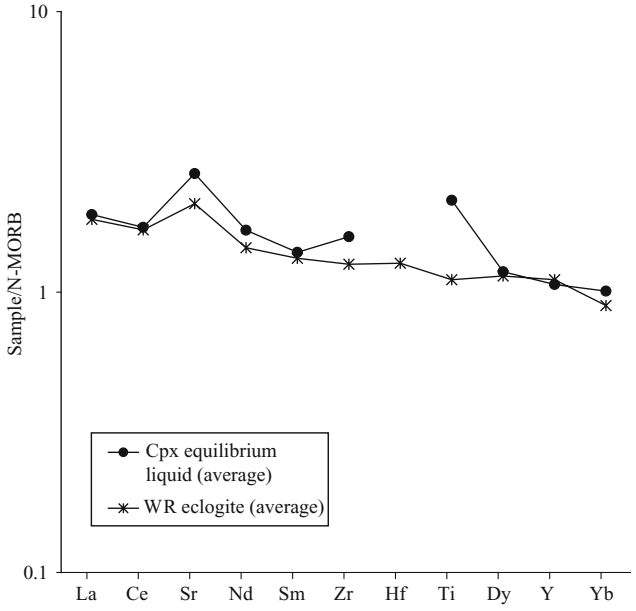

Fig. 11 Trace element (normalised to N-MORB values) of calculated liquids from clinopyroxene (metagabbro) compared to the whole rock compositions of the eclogites (average values)

resetting of the zircon isotope system is variably explained with high-temperature solid-state recrystallisation (Ashwal et al. 1999; Hoskin and Black 2000) or with zircon/fluid interaction during younger metamorphic events (Hartmann 2000). This process may be facilitated by the occurrence of metamict areas in zircon with strongly enhanced isotope mobility. A thermal perturbation related to a younger metamorphic event can promote re-crystallisation of the metamict zones, thereby yielding apparent ages with no geological meaning (Pidgeon 1991; Geisler et al. 2001).

We suggest that the time of crystallisation of the eclogite igneous protolith is reasonably recorded by the older mean concordant age of 468 ± 4 Ma defined by the largest ''igneous'' zircon population. Note that this radiometric date is within error of the inferred emplacement age of the gabbro. The younger ages clustering around the mean value of 446 ± 2 Ma are most likely due to partial isotope mobilisation during the subsequent metamorphic evolution.

The gabbros have high mg# (0.77–0.80) and positive Eu and Sr anomalies in the primordial mantle-normalised multivariation diagram, thus indicating a cumulus origin controlled by clinopyroxene (± olivine) and plagioclase segregation. We calculated the incompatible trace element composition of the melt in equilibrium with the clinopyroxene by applying the clinopyroxene/liquid partition coefficients for a basaltic system (Tiepolo et al. 2002). The MORB-normalised REE patterns of computed melts show no significant LREE enrichment (La_N/Sm_N = 0.8–1.8) and nearly flat HREE profiles.

The Nd isotope compositions at the time of igneous crystallisation were calculated on the basis of the U-Pb zircon data from the present study. The gabbros have initial ε_{Nd} ranging from +5.4 to +8.8. The variability in the initial ε_{Nd} values is most likely related to the interaction of a fractionating melt derived from a depleted mantle source with a low ε_{Nd} crustal component. This is indicated by the fact that the initial ε_{Nd} is roughly correlated with chemical features of clinopyroxene (e.g. it decreases with decreasing mg# and with increasing La_N/Sm_N). We thus propose that the mantle melt evolved through a process controlled by fractionation and concomitant assimilation of crustal material. The crustal contamination process is consistent with the occurrence of staurolite-, garnet- and magnetite-rich fels within the amphibolitised gabbros, which are considered evidence for country rock assimilation during magma emplacement (see also Braga and Tribuzio 1999). The presence of zircons with complex zoning patterns and ages (495–2129 Ma) older than the inferred magma crystallisation age provide further proof of inheritance from a crustal source.

The eclogites differ from the gabbros in their bulk chemical composition. Their chemical fingerprint may be representative of a melt composition and rules out derivation through a cumulus process. The variable mg# (0.51–0.67) and relatively high REE and incompatible element contents (15–35 times typical chondrite values) suggest an origin from evolved melts. The slight LREE depletion (La_N/Sm_N = 0.6 – 0.8) and the Zr/Nb and Y/Nb ratios (33–43 and 10–17, respectively) are consistent with the chemical features of N- or T-MORB. The initial ε_{Nd} of eclogites is similar to that of the analysed gabbros and ranges from +7.0 to +9.2, showing a rough negative correlation with the whole rock La_N/Sm_N ratio. There is good correspondence between the bulk trace element composition of the eclogites and the composition of the melts in equilibrium with the clinopyroxene from the gabbros of cumulus origin (Fig. 11). In addition, the U-Pb zircon ages indicate that the eclogite protoliths and gabbros are coeval (469 ± 6 and 468 ± 4 Ma, respectively). This sustains the hypothesis that the eclogite protoliths and gabbros were cogenetic, i.e. they formed from variably evolved and crustally contaminated melts that were derived from similar depleted mantle sources. The lack of high pressure parageneses in the metagabbros and associated paragneisses suggests that the crustal sections containing the relics of gabbros and eclogites were juxtaposed during the amphibolite facies Variscan evolution. An Alpine juxtaposition of the two

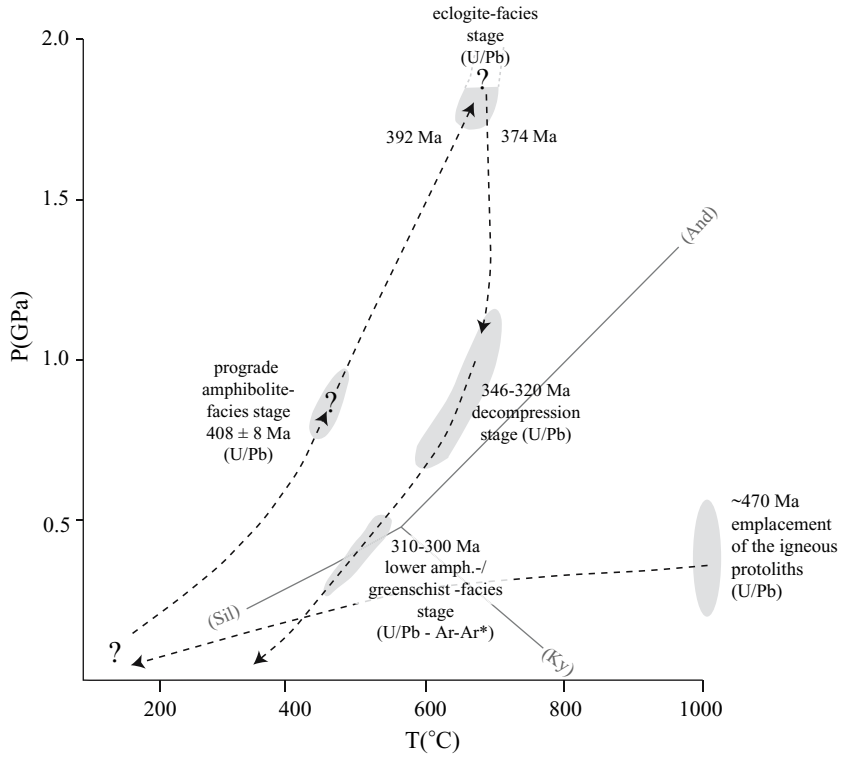

Fig. 12 Schematic P-T-t evolution of the eclogites from the Savona Crystalline Massif (pressure-temperature estimates from Messiga et al. 1992 and Cortesogno et al. 1997). *Ar-Ar data from Barbieri et al. (2003)

sections cannot be demonstrated due to absence of know shear zones or faults in the region of interest.

Cambro-Ordovician magmatism in the western European Variscides

Basic rocks of mid-Ordovician age are not a novelty in portions of the Variscan basement from the western Mediterranean area. The occurrence of mafic rocks with Cambro-Ordovician protoliths has already been reported in the Western-Central Alps, Sardinia and Provençe (Lancelot et al. 1998; Ménot et al. 1988; Paquette et al. 1989; Oberli et al. 1994; Abrecht et al. 1995; Poller 1997; Rubatto et al. 2001; Schaltegger et al. 2003; Cortesogno et al. 2004; Palmeri et al. 2004; Giacomini et al. 2005). Similarly to the Savona crystalline massif, these mafic rocks mostly occur as amphibolite or retrogressed eclogite bodies within paragneiss and orthogneiss sequences, and the protolith ages range from about 495 to 450 Ma. In particular, in-situ U/Pb zircon data (Rubatto et al. 2001; Palmeri et al. 2004; Giacomini et al. 2005) yield ages in the range of 460–450 Ma, which are usually younger than those obtained by conventional methods. These rocks commonly have E- to N-MORB chemical affinity, with initial ε_{Nd} values ranging from +4 to +9. The low ε_{Nd} values are alternatively attributed to processes of crustal contamination (e.g. Paquette et al. 1989) or to an origin in active margin/island-arc environments (Oberli et al. 1994; Schaltegger et al. 2003).

True oceanic crust sequences are scarce in the Variscan chain. In the southern-western portion of the belt they could be represented by the Cambro-Ordovician Chamrousse ophiolite from the Belledonne Massif of the western Alps and possibly by some sequences in the French Maures Massif (Bellot 2005, and references therein). The Chamrousse ophiolite was interpreted as a crustal fragment of an ''immature'' oceanic basin (Guillot et al. 1992 and references therein), in agreement with the lack of pelagic sediments in the stratigraphic cover, which instead contains significant quantities of metatuff (Pin and Carme 1987). Based on conventional U-Pb geochronology applied to zircons from a plagiogranite, the Chamrousse ophiolite was dated at 496 ± 6 Ma (Ménot et al. 1988). The ophiolite has a complex geochemical signature, as the presence of non-cumulitic mafic rocks with variable LREE enrichment and initial ε_{Nd} of +5 to +9 testify (Bodinier et al. 1981; Pin and Carme 1987). The geochemical signature of the Chamrousse sequence was attributed to mixing of N-MORB and E-MORB-like end members with a third component having subduction zone affinity (Pin and Carme 1987).

The protoliths of metagabbros and eclogites from the Savona Crystalline Massif originated from depleted mantle melts emplaced within a continental crust. They

most likely record a process of contamination by crustal material. We have no evidence to sustain the hypothesis of their origin in a supra-subduction or a mid-ocean ridge setting. We propose that the Ligurian Briançonnais basement records a mid-Ordovician extensional phase characterised by intrusion of mantle-derived melts into the continental crust. The widespread occurrence of mantle melts intruding the pre-Variscan crust in the Mediterranean area has been taken as evidence for the development of an oceanic domain at the northern margin of Gondwana (Stampfli and Borel 2002; Stampfli et al. 2002; von Raumer et al. 2003), which marks the beginning of the new Wilson cycle leading to the Variscan orogeny. Considering the scattered occurrence of mafic rocks in the basement outcrops of the southern Variscides and their variable chemical and isotopic fingerprints, we suggest that the Cambro-Ordovician basin did not evolve into a true ocean, but was likely a basin on (thinned?) continental crust.

Timing of Variscan metamorphism in the Ligurian eclogites

Dating the eclogitic peak by means of zircon geochronology is not straightforward, mainly because it is often difficult to relate zircon U-Pb ages to the P-T conditions of metamorphic equilibration. Zircons grown or re-crystallised under eclogite and amphibolite facies conditions may have almost indistinguishable trace element patterns. Their composition (especially HREE and Y) is controlled by the presence of garnet (Rubatto 2002), which often remains stable (or metastable) during decompression to amphibolite-facies conditions. In addition, the common dispersion of ''metamorphic'' ages along the Concordia does not facilitate the interpretation of data and demonstrates that zircon may be an open system under particular metamorphic conditions (e.g. Timmermann et al. 2004; Gray et al. 2004; Giacomini et al. 2005).

In the studied eclogite, the age of zircons younger than the crystallisation age of the inferred igneous protolith and with typical metamorphic texture spans from 420 ± 17 to 305 ± 6 Ma. The zircons with ages of 420 ± 17–402 ± 8 Ma underwent a textural resetting that cancelled the igneous textures: their trace element composition is similar to that of the older igneous zircons (negative Eu anomaly, HREE enriched with respect to LREE and MREE). These grains probably represent a further step in the process of annealing during prograde metamorphism, as already observed in the rejuvenated igneous zircon (mean age of 446 ± 2 Ma) described in the previous paragraphs. The mean concordant age of 407 ± 9 Ma obtained from the four oldest zircons with metamorphic textures is therefore considered a prograde stage of subduction-related metamorphism (amphibolite facies conditions?) which promoted a process of solid-state recrystallisation in zircon. This is consistent with the evidence for prograde metamorphic crystallisation in the Savona eclogites (i.e. hornblende grains within the cores of garnet porphyroblasts) reported by Messiga et al. (1992).

All analysed zircons with ages younger than 392 Ma are texturally and compositionally indistinguishable. They are euhedral to subrounded or mostly anhedral and have flat HREE patterns (generally 10–100 times typical chondrite values) with no negative Eu anomaly, overall low trace element abundances and low Th/U ratios. These zircons were derived from equilibration of igneous zircons or new precipitation in a system containing stable or metastable garnet and in the absence of high modal percentages of plagioclase. In particular, a fractured zircon rim dated at 374 ± 18 Ma contains an inclusion of diopside-plagioclase symplectite, a typical product of omphacite breakdown during decompression. There is no clear evidence to establish whether the zircon enclosed an omphacite crystal during the eclogite peak or a symplectite portion during the early stages of decompression. However, the presence of small fractures around the inclusion could be attributed to an increase in volume related to the omphacite breakdown reaction; in this case, the development of the diopside-plagioclase symplectite post-dated the measured zircon age. Following this hypothesis, the seven ages ranging from 392 ± 7 to 374 ± 8 Ma are related to equilibration under eclogite-facies conditions.

The trace-element patterns of zircons with ages in the 346–320 range (giving a mean Concordia age at 333 ± 7 Ma) are similar to those of older metamorphic zircons and are typical of growth or re-crystallisation in the presence of garnet. The comparison with published data on the neighbouring Variscan outcrops of the western Alps and Sardinia supports the notion that the zircons younger than 350 Ma are related to post-eclogite exhumation. The exhumation of high-pressure rocks and the process of nappe stacking related to the main continental collision are constrained to about 350–310 Ma by different geochronological methods (Ferrara et al. 1978; Rubatto et al. 2001; Di Vincenzo et al. 2004; Palmeri et al. 2004; Giacomini et al. 2005; Giacomini et al. 2006). We therefore propose that the flat HREE patterns of these zircons are linked either to the presence of stable-metastable garnet in the post-eclogitic assemblages or to the inefficiency of the

re-crystallisation process in completely erasing the trace element signature of older ''eclogitic'' zircons.

One thin rim (no trace element composition for this spot) yielded a young concordant age of 305 ± 6 Ma. This age is consistent with available geochronological data for amphibolite facies equilibration recorded by associated paragneisses and orthogneisses, which indicate 327–297 Ma (Del Moro et al. 1981; Barbieri et al. 2003). We conclude that such a young zircon rim from the selected eclogite is related to late-stage growth during the final stages of exhumation.

The pre-Alpine metamorphic history: a regional comparison

The U/Pb age distribution in the selected eclogite of the Savona Crystalline Massif further constrains the Palaeozoic metamorphic evolution of the European Variscan belt in the Mediterranean area. For the first time in this sector of the chain, the high-pressure metamorphic overprint has been dated to 392–374 Ma. The post-eclogitic evolution is recorded by several zircon ages that yield a mean Concordia age of 333 ± 7 Ma. These new ages are complementary to previously published data (Rubatto et al. 2001; Cortesogno et al. 2004; Palmeri et al. 2004; Giacomini et al. 2005) on high-pressure rocks in the basements of Sardinia and the Western Alps. All these eclogite relics have similar geological settings and peak parageneses, and mainly occur as lenses and boudins within dominant amphibolite-facies paragneiss and orthogneiss sequences.

In northern Sardinia, SHRIMP and LA-ICP-MS U-Pb zircon data constrain the post-eclogite exhumation stage (granulite- to amphibolite-facies) from about 350 to 320 Ma (Palmeri et al. 2004; Giacomini et al. 2005). New data on two samples of kyanite-bearing eclogites from the Sardinian basement (Giacomini et al. unpublished) confirm the presence of a dominant metamorphic zircon population with ages spanning from 367 to 301 Ma. In the external massifs of the western Alps (Belledonne and Argentera), high-pressure metamorphism occurred from 425 to 395 Ma (conventional U/Pb zircon dilution, Paquette et al. 1989). In addition, muscovite Ar-Ar ages of 375–350 Ma for the Argentera Massif were attributed to the amphibolite-facies retrograde overprint (Monié and Maluski 1983). In the same area, however, SHRIMP and ID-TIMS U/Pb zircon ages from an eclogitised metagabbro (Rubatto et al. 2001) indicate that the post-eclogite amphibolitic overprint occurred at 323 ± 3 Ma. Older metamorphic ages (~470 Ma) were proposed by Gebauer et al. (1988) and Oberli et al. (1994) for some eclogites cropping out in the Aar-Gotthard massif (central Alps). On the basis of an upper intercept discordia age at 870 Ma, Gebauer et al. (1988) proposed that these eclogites have igneous protoliths of Precambrian age and that the eclogite-facies overprint refers to Caledonian accretion.

Geochronological estimates from the western Alps and Sardinia constrain the beginning of the Variscan prograde metamorphic evolution to Siluro-Devonian times. The broad time span proposed for eclogite facies equilibration (425–375 Ma) can be attributed to either diachronous subduction in the different zones, or to uncertainties related to the application of different dating methods. We favour the latter hypothesis, in agreement with the complex internal features and the domains with different U/Pb ages observed in metamorphic zircons through recent micro-analytical studies (e.g. Rubatto et al. 1999; Song et al. 2005; Giacomini et al. 2006; this work). In addition, the different areas yield consistent post-eclogite U/Pb zircon datings at 340–320 Ma, which are commonly interpreted as the timing of amphibolite facies equilibration at middle crustal levels (Rubatto et al. 2001; Di Vincenzo et al. 2004; Palmeri et al. 2004; Giacomini et al. 2005; Giacomini et al. 2006). Thus, old ''eclogitic'' ages like proposed in the Belledonne and the Argentera massifs would imply very slow rates (0.6–0.4 mm/year) to exhume the high pressure rocks to the middle crustal levels (~0.5 GPa) inferred for the widespread amphibolite facies overprint. Exhumation rates are almost 1.5- to 2-fold quicker (0.9–1 mm/a) if calculated taking into account the youngest eclogitic ages proposed in this contribution.

Conclusions

The Savona Crystalline Massif was intruded at ~468 Ma by basaltic melts that originated from depleted mantle sources, probably in response to regional Cambro-Ordovician crustal extension at the northern margin of Gondwana. The mantle melts underwent fractional crystallisation and crustal contamination in relation to their emplacement in the continental crust.

In Devonian times at least part of the Savona Crystalline Massif was involved in a subduction zone that produced eclogite-facies assemblages pointing to equilibration at minimum pressures of 1.7 GPa and temperatures of 650–750 °C (Fig. 12). In particular, LA-ICP MS analyses of metamorphic zircons from one eclogite show that the high-pressure metamorphic overprint occurred between 392 and 374 Ma. Based on a comparison with other published data, the younger ages of metamorphic zircons that cluster around a

mean Concordia age of 333 ± 6 Ma (i.e. in the Late Carboniferous) are ascribed to the amphibolite facies overprint related to the main Variscan collision and the chain exhumation.

The present study also shows that the U/Pb isotope system in zircons from eclogites is a powerful tool for reconstructing the chronology of entire orogenic cycles. Within a single eclogite sample from the Variscan Savona Massif, the evaluation of U-Pb zircon microanalyses in association with CL images and trace element signatures allowed us to identify five petrogenetic events: (1) old zircons inherited from the pre-Variscan basement, (2) igneous zircons dating the crystallisation of the eclogite protolith during an extensional tectonic event, (3) variably rejuvenated zircons, at least partly related to a prograde metamorphic stage which marked the onset of plate convergence, (4) peak eclogitic zircons dating the involvement of the crustal slice at deep subduction levels, and (5) retrograde zircons associated with eclogite exhumation under amphibolite facies conditions in response to continental collision.

Acknowledgments We are grateful to Bruno Messiga that in different times introduced us to the geology of the Savona Crystalline Massif. Angela Ivaldi and Stefano Maffeo are also acknowledged for precious help in the field. Special thanks are due to Claudio Ghezzo for stimulating discussions. Suggestions and comments by Felix Oberli and an anonymous referee led to a considerable improvement of the original manuscript. This work was financially supported by Ministero dell'Università e della Ricerca Scientifica (Progetti di Ricerca di Interesse Nazionale, Ghezzo and Tribuzio fundings).

References

Abrecht J, Biino GG, Schaltegger U (1995) Building the European continent: Late Proterozoic– Early Paleozoic accretion in the Central Alps of Switzerland. Terra Abstracts 7(1):105–105

van Achterbergh E, Ryan CG, Jackson SE, Griffin W (2001) Data reduction software for LA-ICP-MS. In Laser ablation-ICPMS in the earth science. P. Sylvester ed. Mineralogical Association of Canada. vol. 29:239–243

Ashwal LD, Tucker RD, Zinner Ek (1999) Slow cooling of deep crustal granulites and Pb-loss in zircon. Geochimica et Cosmochimica Acta 63(18):2839–2851

Barbieri C, Carrapa B, Di Giulio A, Wijbrans J, Murrell GR (2003) Provenance of Oligocene synorogenic sediments of the Ligurian Alps (NW Italy): inferences on belt age and cooling history. Int J Earth Sci 92:758–778

Bea F, Montero P (1999) Behaviour of accessory phases and redistribution of Zr, REE, Y, Th and U during metamorphism and partial melting of metapelites in the lower crust: an example from the Kinzigite Formation of Ivrea-Verbano, NW Italy. Geochim Cosmochim Acta 63:1133–1153

Bellot J (2005) The Palaeozoic evolution of the Maures massif (France) and its potential correlation with others areas of the Variscan belt: a review. J Virtual Explor, 19

Bodinier JL, Dupuy G, Dostal J, Carme F (1981) Geochemistry of ophiolites from the Chamrousse complex (Belledonne massif, Alps). Contrib Mineral Petrol 78 (379–388)

Braga R, Tribuzio R (1999) Late-Variscan amphibolitisation of gabbroic rocks from the Brianconnais basement (Savona Crystalline Massif, Western Alps). Plinius 22:67–68

Cortesogno L, Dallagiovanna G, Gaggero L, Vanossi M (1993) Elements for the Palaeozoic history of the Ligurian alps. In: von Raumer J, Neubauer, F (eds) Pre-Alpine Geology in the Alps, vol. Springer, Berlin Heidelberg New York: 257–277

Cortesogno L, Gaggero L, Capelli C (1997) Petrology of pre-Alpine eclogites and amphibolites from the Ligurian Brianconnais basement. Atti Ticinensi Scienze della Terra 39:3–29

Cortesogno L, Gaggero L, Oggiano G, Paquette JL (2004) Different tectono-thermal evolutionary paths in eclogitic rocks from the axial zone of the Variscan Chain in Sardinia (Italy) compared with the Ligurian Alps. Ofioliti 29(2):125–144

Del Moro A, Pardini G, Messiga B, Poggio M (1981) Dati petrologici e radiometrici preliminari sui massicci cristallini della Liguria occidentale. Rendiconti Società Italiana di Mineralogia e Petrologia 38(1):73–87

Di Vincenzo G, Carosi R, Palmeri R (2004) The relationship between tectono-metamorphic evolution and argon isotope records in white micas: constraints from in situ 40Ar–39Ar laser analysis of the Variscan basement of Sardinia (Italy). J Petrol 45:1013–1043

Ferrara G, Rita F, Ricci CA (1978) Isotopic age and tectono-metamorphic history of the metamorphic basement of North-eastern Sardinia. Contrib Mineral Petrol 68:99–106

Gaggero L, Cortesogno L, Bertrand JM (2004) The pre-Namurian basement of the Ligurian Alps: a review of the lithostratigraphy, pre-Alpine metamorphic evolution, and regional comparison. Periodico di Mineralogia 73(2):85–96

Gebauer D (1993) Isotopic systems - geochronology of eclogites. In: D.A C (ed) Eclogite facies rocks, vol. Blackie, Glasgow: 132–159

Gebauer D, Quadt A, Compston W, Williams IS, Grünefelder M (1988) Archaean zircons in a retrograded, Caledonian eclogite of the Gotthard Massif (Central Alps, Switzerland). Schweizerische Mineralogische Petrographische Mitteilungen 68:485–490

Geisler T, Pidgeon RT, van Bronswijk w, Pleysier R (2001) Kinetics of thermal recovery and recrystallization of partially metamict zircon: a Raman spectroscopic study. Eur J Mineral 13(6):1163–1176

Giacomini F, Bomparola RM, Ghezzo C (2005) Petrology and geochronology of metabasites with eclogite facies relics from NE Sardinia: constraints for the Palaeozoic evolution of Southern Europe. Lithos 82:221–248

Giacomini F, Bomparola RM, Ghezzo C, Guldbrandsen H (2006) The geodynamic evolution of the Southern European Variscides: constraints from the U/Pb geochronology and geochemistry of the lower Palaeozoic magmatic-sedimentary sequences of Sardinia (Italy). Contrib Mineral Petrol 86:19–42

Gray DR, Hand M, Mawby J, Armstrong RA, McL. Miller J, Gregory RT (2004) Sm–Nd and Zircon U–Pb ages from garnet-bearing eclogites, NE Oman: constraints on High-P metamorphism. Earth Planet Sci Lett 222:407–422

Guillot S, Ménot RP, Lardeaux JM (1992) Techtonique intra-océanique distensive dans l'ophiolite paléozoique de Chamrousse (Alpes occidentales). Bulletin Société Géologique de France 163(3):229–240

Hartmann LA, Leite JAD, Da Silva LC, Remus MVD, McNaughton NJ, Groves DI, Fletcher IR, Santos JOS, Vasconcellos MAZ (2000) Advances in SHRIMP geochronology and their impact on understanding the tectonic and metallogenic evolution of southern Brazil. Aust J Earth Sci 47(5):829–844

Hoskin PWO, Black LP (2000) Metamorphic zircon formation by solid-state recrystallization of protolith igneous zircon. J Metamorphic Geol 18(4):423–439

Ketchum JWF, Jackson SE, Culshaw NG, Barr SM (2001) Depositional and tectonic setting of the Paleoproterozoic Lower Aillik Group, Makkovik Province, Canada: evolution of a passive margin–foredeep sequence based on petrochemistry and U-Pb (TIMS and LAM-ICP-MS) geochronology: Precambrian Res 105:331–356

Lancelot J, Moussavou M, Delor C (1998) Géochronologie U/Pb des témoins de l'evolution ante-varisque du Massif des Maures. Geologie du Massif des Maures – Réunion Spécialisée BRGM. Societé Géologique de France, Le Plan de la Tour, 20.Mai 1998, p 22

Ludwig KR (1999) Isoplot/Ex version 2.00: A geochronological toolkit for microsoft excel. Berkeley Geochronology Center Special Publications 1a. 46 pp

Ménot RP, Peucat JJ, Scarenzi D, Piboule M (1988) 496 Ma age of plagiogranites in the Chamrousse ophiolite complex (external crystalline massifs in the French Alps): evidence of a lower Palaeozoic oceanization. Earth Planetary Sci Lett 88:82–92

Messiga B (1987) Alpine metamorphic evolution of Ligurian Alps (North-West Italy): chemography and petrological constraints inferred from metamorphic climax assemblages. Contrib Mineral Petrol 95:269–277

Messiga B, Tribuzio R, Caucia F (1992) Amphibole evolution in Variscan eclogite-amphibolites from the Savona crystalline massif (western Ligurian Alps, Italy). Controls on the decompressional P-T-t path. Lithos 27:215–230

Miller C, Konzett J, Tiepolo M, Armstrong RA, Thöni M (2006) Jadeite-gneiss from the Eclogite zone Tauern Window, Easter Alps, Austria. Metamorphic, geochemical and zircon record of a sedimentary protolith. Lithos (in press)

Monié P, Maluski H (1983) Données géochronologiques 39Ar-40Ar sur le socle anté-Permien du massif de l'Argentera-Mercantour (Alpes Maritimes, france). Bulletin Société Géologique de France 2:247–257

Oberli F, Meier M, Biino GG (1994) Time constraints on the pre-Variscan magmatic/metamorphic evolution of the Gotthard and Tavetsch units derived from single-zircon U-Pb results. Schweizerische Mineralogische Petrographische Mitteilungen 74:483–488

Palmeri R, Fanning M, Franceschelli M, Memmi I, Ricci CA (2004) SHRIMP dating of zircons in eclogite from the Variscan basement in north-eastern Sardinia (Italy). Neues Jahrbuch Mineralogie Abh 6:275–288

Paquette JL, Menot RP, Peucat JJ (1989) REE, Sm-Nd and U-Pb zircon study of eclogites from the Alpine External Massifs (Western Alps): evidence for crustal contamination. Earth Planetary Sci Lett 96:181–198

Pidgeon RT (1991) Recrystallisation of oscillatory zoned zircon: some geochronological and petrological implications. Contrib Mineral Petrol 110(4):463–472

Pin C, Carme F (1987) A Sm-Nd isotopic study of the 500 Ma old oceanic crust in the Variscan belt of western Europe: the Chamrousse ophiolite complex, Western Alps (France). Contrib Mineral Petrol 196:406–413

Poller U (1997) U–Pb single-zircon study of gabbroic and granitic rocks in the Val Barlas-ch (Silvretta nappe, Switzerland). Schweizerische Mineralogische Petrographische Mitteilungen 77:351–360

von Raumer J, Stampfli GM, Bussy F (2003) Gondwana derived microcontinents - the constituents of the Variscan and Alpine collisional orogens. Tectonophysics 365:7–22

Rubatto D (2002) Zircon trace element geochemistry: partitioning with garnet and the link between U-Pb ages and metamorphism. Chem Geol 184(1):123–138

Rubatto D, Gebauer D (2000) Use of cathodoluminescence for U-Pb zircon dating by ion microprobe: some examples from the Western Alps. In: Pagel M, Barbin V, Blanc P, Ohnenstetter D (eds) Cathodoluminescence in Geosciences. Springer, Berlin Heidelberg New York, pp 373–400

Rubatto D, Schaltegger U, Lombardo B, Colombo F, Compagnoni R (2001) Paleozoic magmatic and metamorphic evolution of the Argentera Massif (Western Alps) resolved with U-Pb dating. Schweizerische Mineralogische Petrographische Mitteilungen 81(2):213–228

Rubatto D, Gebauer D, Compagnoni R (1999) Dating of eclogite-facies zircons: the age of Alpine metamorphism in the Sesia-Lanzo Zone (Western Alps). Earth and Planet Sci Lett 167:141–158

Schaltegger U, Fanning CM, Günther D, Maurin JC, Schulmann K, Gebauer D (1999) Growth, annealing and recrystallization of zircon and preservation of monazite in high-grade metamorphism; conventional and in-situ U-Pb isotope, cathodoluminescence and microchemical evidence. Contrib Mineral Petrol 134:186–201

Schaltegger U, Abrecht J, Corfu F (2003) The Ordovician orogeny in the Alpine basement: constraints from geochronology and geochemistry in the Aar Massif (Central Alps). Swiss Bull Mineral Petrol 83(2):183–239

Song S, Zhang L, Niu Y, Su L, Jian P, Liu D (2005) Geochronology of diamond-bearing zircons from garnet peridotite in the North Qaidam UHPM belt, Northern Tibetan Plateau: A record of complex histories from oceanic lithosphere subduction to continental collision. Earth Planet Sci Lett 234:99–118

Stampfli GM, Borel GD (2002) A plate tectonic model for the Paleozoic and Mesozoic constrained by dynamic plate boundaries and restored synthetic oceanic isochrons. Earth Planet Sci Lett 196:17–33

Stampfli GM, von Raumer J, Borel G (2002) The Palaeozoic evolution of pre-Variscan terranes: from Gondwana to the Variscan collision. In: Martinez Catalan JR, Hatcher RD, Arenas R, Diaz Garcia F (eds) Variscan-Appalachian dynamics: the building of late Palaeozoic basement, Geological Society of America, Special Paper 364:263–280

Tiepolo M (2003) In situ Pb geochronology of zircon with laser ablation–inductively coupled plasma–sector field mass spectrometry. Chem Geol 192:1–19

Tiepolo M, Tribuzio R, Vannucci R (2002) The composition of mantle-derived melts developed during the Alpine continental collision. Contrib Mineral Petrol 144:1–15

Timmermann H, Stedra V, Gerdes A, Noble SR, Parrish RR, Dörr W (2004) The Problem of Dating High-pressure Metamorphism: a U–Pb Isotope and Geochemical Study on Eclogites and Related Rocks of the Mariànské Lazne Complex, Czech Republic. J Petrol 45(7):1311–1338

Tribuzio R, Tiepolo M, Vannucci R, Bottazzi P (1999) Trace element distribution within olivine-bearing gabbros from the Northern Apennine ophiolites (Italy): evidence for post-cumulus crystallisation in MOR-type gabbroic rocks. Contrib Mineral Petrol 134:123–133

Tribuzio R, Thirlwall MF, Vannucci R (2004) Origin of the Gabbro–Peridotite Association from the Northern Apennine Ophiolites (Italy). J Petrol 45(6):1109–1124

Vanossi M, Cortesogno L, Galbiati B, Messiga b, Piccardo GB, Vannucci R (1984) Geologia delle Alpi Liguri: dati, problemi, ipotesi. Memorie società Geologica Italiana 28:5–75